

# LEARNING COLLECTIVE VARIABLES FROM BIOEMU WITH TIME-LAGGED GENERATION

**Seonghyun Park<sup>1</sup>, Kiyoung Seong<sup>1</sup>, Soojung Yang<sup>2</sup>, Rafael Gómez-Bombarelli<sup>2</sup>, Sungsoo Ahn<sup>1†</sup>**  
 Korea Advanced Institute of Science and Technology (KAIST)<sup>1</sup>,  
 Massachusetts Institute of Technology (MIT)<sup>2</sup>,  
 {hyun26, kyseong98, sungsoo.ahn}@kaist.ac.kr,  
 {soojungy, rafagb}@mit.edu

## ABSTRACT

Molecular dynamics is crucial for understanding molecular systems, but its applicability is often limited by the vast timescales of rare events like protein folding. Enhanced sampling techniques overcome this by accelerating the simulation along key reaction pathways, which are defined by collective variables (CVs). However, identifying effective CVs that capture the slow, macroscopic dynamics of a system remains a major bottleneck. This work proposes a novel framework coined BIOEMU-CV that learns these essential CVs automatically from BioEmu, a recently proposed foundation model for generating protein equilibrium samples. In particular, we re-purpose BioEmu to learn time-lagged generation conditioned on the learned CV, i.e., predict the distribution of molecular states after a certain amount of time. This training process promotes the CV to encode only the slow, long-term information while disregarding fast, random fluctuations. We validate our learned CV on fast-folding proteins with two key applications: (1) estimating free energy differences using on-the-fly probability enhanced sampling and (2) sampling transition paths with steered molecular dynamics. Our empirical study also serves as a new systematic and comprehensive benchmark for MLCVs on fast-folding proteins larger than Alanine Dipeptide.

## 1 INTRODUCTION

Many problems in biomolecules reduce to understanding the complex behavior of how molecules move and change conformations, such as estimating the drug-target binding affinities (De Vivo et al., 2016; Abel et al., 2017) or the folding time of proteins (Piana et al., 2012; Spotte-Smith et al., 2022). Molecular dynamics (MD) simulation is one of the principal ways to study the movements in molecular systems, describing the microscopic movements by integrating differential equations with femtosecond ( $10^{-15}$ ) time step. However, events like protein folding often happen in a much larger time-scale, from microseconds ( $10^{-6}$ ) to milliseconds ( $10^{-3}$ ). Due to this timescale gap, observing desired events in naive MD requires integrating over computationally infeasible number of step, which is considered unrealistic for most real world problems.

To overcome this timescale limitation, various enhanced sampling techniques have been studied (Hénin et al., 2022). Metadynamics (Barducci et al., 2011) applies biasing force to the molecular systems to encourage transitions, while replica-exchange MD (Sugita & Okamoto, 1999) exchanges configurations between parallel simulations at different temperatures. Also, accelerated MD (Hamelberg et al., 2004) globally boosts the potential energy surface to overcome energy barriers. Their core idea is to add biasing forces throughout the simulation to guide exploration and transitions in the molecular state space, without breaking the equilibrium conditions. Importantly, this biasing forces are computed based on a low-dimensional representation, denoted as the *collective variables* (CVs). Therefore, CVs well encoding the slow degree of freedom will add biases to numerously seen CVs, resulting exploration and transition to unseen and less visited states.

However, CVs have been mainly hand-crafted by domain expertise, e.g., selection of specific backbone dihedral angles for Alenine Dipeptide, which may miss slow modes and has been limited to small systems. To resolve this issue, several works have considered machine-learned CVs (ML-

CVs) from MD trajectory data. Supervised methods use ground-truth state definitions and pseudo-labels (Bonati et al., 2020; Trizio & Parrinello, 2021), while self-supervised methods rely on time-lagged data to encode the dynamics information (Bonati et al., 2021; Wehmeyer & Noé, 2018; Hernández et al., 2018). While prior works have shown promising results on small systems such as alanine dipeptide, they currently lack the ability to scale to larger systems such as proteins and lack standardized, side-by-side systematic comparison.

In this work, we present a simple yet efficient framework for learning collective variables (CVs) from the latent representation of a molecular foundation model. Inspired by recent research extracting condition representations from text-to-image diffusion models (Zhang et al., 2023; Mou et al., 2024), we train an MLCV encoder to learn the latent representations in an existing molecular foundation model, BioEmu (Lewis et al., 2025). Building upon its capability of generating multiple protein conformations, we condition time-lagged data and use them as CVs for enhanced sampling techniques. Additionally, we benchmark prior MLCVs on three fast-folding proteins for two downstream tasks by enhanced sampling simulations along with extensive qualitative analysis.

To summarize, our contribution is as follows:

- We propose a framework extracting collective variables from the time-lagged condition representations of a frozen foundation model.
- We extensively benchmark MLCVs with two downstream tasks for the slow degree of freedom: free energy difference estimation and transition path sampling for proteins in explicit water solvent simulations. Furthermore, we demonstrate that our BIOEMU-CV shows competitive performance in these tasks as well as meta-stable state discrimination.

## 2 BACKGROUND

**Molecular dynamics (MD).** MD simulations model the time evolution of molecular systems through atomic coordinates and velocities. An illustrative MD is the underdamped Langevin dynamics (Bussi & Parrinello, 2007) as follows:

$$dx_t = v_t dt, \quad dv_t = \frac{-\nabla U(x_t)}{m} dt - \gamma v_t dt + \sqrt{\frac{2\gamma k_B T}{m}} dW_t,$$

where  $x_t$  and  $v_t$  are atomic positions and velocities,  $m$  is the mass,  $U(x_t)$  the potential energy, and  $-\nabla U(x_t)$  the force. The parameters  $\gamma$ ,  $k_B$ ,  $T$ , and  $W_t$  denote the friction coefficient, Boltzmann constant, temperature, and Brownian motion, respectively. While MD simulations provide atomic-level insights into dynamic process, it remains limited by timescales. The high energy barriers between states makes rare events difficult to observe such as transition paths, often requiring unrealistic long MD simulations (Valsson et al., 2016).

**Enhanced sampling and collective variables (CVs).** To overcome the timescale limitations of the standard MD simulations, enhanced sampling methods introduce biasing forces or potentials to accelerate transitions. Popular approaches include metadynamics (Barducci et al., 2011, MTD), well-tempered metadynamics (Barducci et al., 2008, WTM), replica-exchange molecular dynamics (Hukushima & Nemoto, 1996, REMD), and on-the-fly probability enhanced sampling (Invernizzi & Parrinello, 2020, OPES). These methods typically rely on a low-dimensional descriptors known as *collective variables* (CVs), which serve as a biasing coordinate in the simulation (Bonati et al., 2023). Formally, the CVs, denoted by  $c$ , is represented as a set of functions of atomic position  $x$ :

$$c(x) = [\xi_1(x), \dots, \xi_d(x)],$$

where  $d \ll 3N$  is the number of CVs. In this work, we fix the dimensionality to one for simplicity and visibility. CVs are designed to capture the system’s slow degree of freedom, often chosen based on domain knowledge, such as specific backbone dihedral angles or inter-residue contact distances (Piana & Laio, 2007). However, handcrafted CVs remain mostly limited to small systems (Pietrucci & Laio, 2009; Noé & Clementi, 2017).

**Machine-learned collective variables (MLCVs).** Recent methods employ machine learning to automatically identify CVs beyond handcrafted features. Supervised approaches such as DeepLDA (Bonati et al., 2020) and DeepTDA (Trizio & Parrinello, 2021) learn CVs through discriminant analysis. However, they require predefined binary state labels, where one needs to specify a representative folded state and choose an RMSD threshold for classification. In contrast,

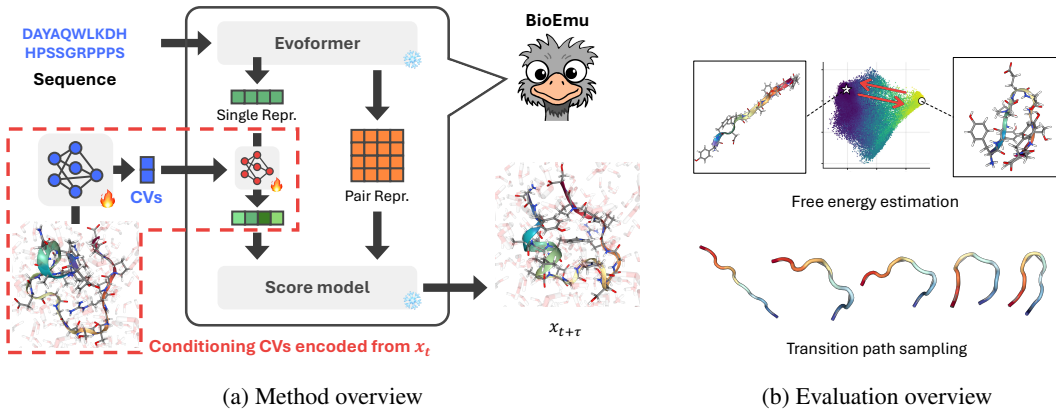


Figure 1: **Overview of our framework and evaluation simulation.** (**Left**) We train an encoder on top of the conditions of a frozen molecular foundation model to learn collective variables (CVs) for protein, highlighted in red dotted lines, on top of a frozen pre-trained BioEmu. (**Right**) Two downstream tasks for the slow degree of freedom, free energy estimation and transition path sampling.

self-supervised and time-lagged methods instead leverage dynamical information from trajectories. DeepTICA (Bonati et al., 2021) applies time-lagged independent component analysis (Molgedey & Schuster, 1994, TICA) as a loss for encoded representations. The time-lagged autoencoder (Wehmeyer & Noé, 2018, TAE) and variational dynamics encoder (Hernández et al., 2018, VDE) reconstructs future configurations  $x_{t+\tau}$  from the present configuration  $x_t$ , deriving latent representations as CVs using autoencoders (Rumelhart et al., 1985) and variational autoencoders (Kingma & Welling, 2014), respectively. However, existing methods mostly focus on small systems such as alanine dipeptide, and systematic comparisons across approaches are absent.

### 3 METHOD

**Overview.** We aim to learn an encoder that outputs a low-dimensional vector representing the slow degree of freedom in molecules, known as collective variables (CVs). Inspired by recent works on conditioning frozen foundation models (Zhang et al., 2023; Mou et al., 2024), we re-purpose the BioEmu model. As shown in Figure 1a, instead of using it for its original purpose of generating protein conformation ensemble, we add an encoder to extract its low dimensional representation to serve as CV, which we call BIOEMU-CV. This CV learns the slow dynamics by approximating the molecular dynamics (MD) propagator with a conditional generative model, which generates a subsequent state from a current state and a time lag similar to Hernández et al. (2018).

**Task formulation.** Given a protein configuration represented by atomic coordinates in  $x \in \mathbb{R}^{N \times 3}$  where  $N$  is the number of atoms, our goal is to learn an encoder  $f_\theta$  that maps the high-dimensional structure into a *low-dimensional representation*  $c = f_\theta(x) \in \mathbb{R}^d$  with  $d \ll 3N$ . This representation, the CVs, should qualify three criteria for the use of enhanced samplings: (i) being low-dimensional, (ii) capturing the system’s slow degree of freedom, and (iii) discriminating the folded and unfolded states in protein (Fu et al., 2024). We fit the first criteria by using a one-dimensional CV, and evaluate the meta-stable state discrimination with secondary structures which are highly correlated to the folded states. For the second and most important criterion, we evaluate MLCVs with two downstream tasks requiring to encode the slow degree of freedom: (i) free energy estimation and (ii) transition path sampling, each by different enhanced sampling techniques.

**Biomolecular Emulator (BioEmu).** BioEmu (Lewis et al., 2025) generates the conformational ensemble at full-atom resolution unlike structure prediction models such as AlphaFold (Jumper et al., 2021), which return a single low-energy conformation given a protein sequence. We focus on the capability to generate protein conformation ensemble, and re-purpose it for learning collective variables (CVs). Formally, given an amino acid sequence  $A = [A_1, A_2, \dots, A_n]$  of length  $n$ , BioEmu is a sequence-conditioned denoising diffusion model  $g_\phi(x|A)$  to sample from the equilibrium distribution  $p(x|A)$ . To be specific, the protein sequence encoder of the BioEmu produces two represen-

Table 1: Quantitative results of 1  $\mu$ s OPES simulations for three fast-folding proteins in explicit water solvent. We report the reference free energy difference ( $\Delta F_{\text{ref}}$ ) from the full dataset, the average free energy difference ( $\Delta F$ ) from simulations, the absolute error between two energy values ( $|\Delta F_{\text{ref}} - \Delta F|$ ), and the potential of mean force (PMF) MAE. Results are averaged over four simulations for Chignolin, and three simulations for Trp-cage and BBA. We mark not applicable (N/A) for CVs that fail at meta-stable state discrimination or show a different sign with the reference value.

Molecule	Method	$\Delta F_{\text{ref}}$	$\Delta F$	$ \Delta F_{\text{ref}} - \Delta F  (\downarrow)$	PMF MAE ( $\downarrow$ )
Chignolin	DeepTICA	-3.73	$-2.02 \pm 3.65$	1.71	$2.64 \pm 3.80$
	TAE	-3.79	$-1.26 \pm 3.69$	2.53	$3.15 \pm 2.81$
	VDE	-17.24	$0.24 \pm 5.00$	N/A	$4.09 \pm 3.20$
	BIOEMU-CV	-3.71	$-3.19 \pm 3.97$	0.52	$3.07 \pm 2.53$
Trp-cage	DeepTICA	3.70	$6.53 \pm 7.31$	2.73	$8.94 \pm 7.43$
	TAE	-1.45	$8.74 \pm 1.65$	N/A	$9.32 \pm 3.91$
	VDE	0.07	N/A	N/A	N/A
	BIOEMU-CV	4.15	$5.97 \pm 3.01$	1.82	$6.86 \pm 4.38$
BBA	DeepTICA	2.76	$13.95 \pm 13.28$	11.19	$10.51 \pm 5.85$
	TAE	-2.88	$-5.46 \pm 4.42$	N/A	$9.97 \pm 3.68$
	VDE	-2.74	N/A	N/A	N/A
	BIOEMU-CV	2.77	$9.99 \pm 5.43$	7.22	$8.34 \pm 7.46$

tations from the amino acid token with Evoformer (Jumper et al., 2021): the single representations  $h := \{h_i\}_{i=1}^N$  and the pair representations  $z := \{z_{ij}\}_{i,j=1}^N$  where  $i, j$  refer to the amino acid index. Based on these two representations, the score model  $g_\phi$  generates  $\alpha$ -carbon ( $C_\alpha$ ) coordinates and residue orientations for the protein backbone. Side chains are then reconstructed using the hpacker package (Visani et al., 2024), followed by short molecular dynamics (MD) simulations for energy relaxation with OpenMM (Eastman et al., 2017).

**Extracting CVs from foundation model.** Recent advances in generative models demonstrate that additional condition encoders with lightweight adapters can be trained on top of unconditional generative models for external guidance (Zhang et al., 2023; Mou et al., 2024). Inspired by this line of research, we propose a framework for using a low-dimensional encoder output as collective variables (CVs); an overview is shown in Figure 1. We train an encoder  $f_\theta$  that maps a configuration  $x$  at time  $t$  to a low-dimensional vector, i.e.,  $c_t = f_\theta(x_t) \in \mathbb{R}^d$ . Then, we fuse the encoded representation to the single representation  $h$  using a small MLP to preserve dimensionality to the score model and keep the adapter lightweight (Zhang et al., 2023). The conditioned representation  $h_t = \text{MLP}(h, c_t)$  and pair representation  $z$  are passed to the score model to generate protein conformations.

**Learning CVs from time-lagged generation.** With this condition pathway in place, we encode CVs of the current conformation but guide the model to generate the time-lagged conformation  $x_{t+\tau}$ , i.e., the score model generates the time-lagged state  $x_{t+\tau}$  from the CVs  $c_t$  with a time lag  $\tau$ . Intuitively, the CV  $c_t$  compresses the information that is shared across  $x_t$  and  $x_{t+\tau}$ , i.e., the slow degree of freedom, while disregarding fast and randomly fluctuating information that is present in the current state  $x_t$  but not in the time-lagged state  $x_{t+\tau}$ . Note that our training objective shares the motivation with VDE (Hernández et al., 2018), but we use a scalable diffusion model architecture and do not need the auto-correlation loss.

To keep the training lightweight, we freeze parameters  $\phi$  of BioEmu, and update the encoder and the conditioning MLP via the denoising score-matching objective (Song et al., 2020; Yim et al., 2021):

$$\mathcal{L}(x_t, x_{t+\tau}, A) = \mathbb{E}_{s \sim \mathcal{U}[0,1]} \left[ \lambda_s \left\| \nabla \log p_{s|0} \left( x_{t+\tau}^{(s)} | x_{t+\tau}^{(0)}, x_t, A \right) - g_\phi(s, h_t, z) \right\|^2 \right], \quad (1)$$

where  $s$  is the diffusion time,  $p_{s|0}$  is the density of  $x_{t+\tau}^{(s)}$  given  $x_{t+\tau}^{(0)}, x_t, A$ ,  $\lambda_s > 0$  the time scheduling weights, and  $g_\phi$  the BioEmu’s score network. This time-lagged reconstruction forces  $c_t$  to capture the slow degree of freedom by incorporating future time-lagged conformation  $x_{t+\tau}$  from the trajectory data, thereby producing CVs suitable for enhanced sampling.

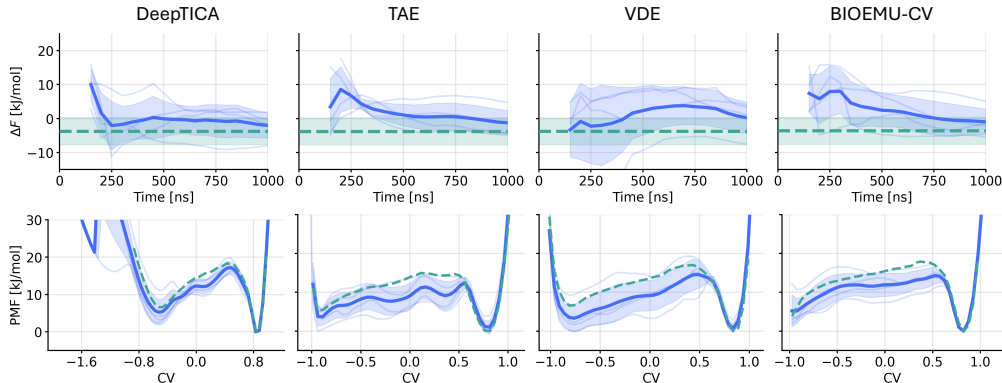


**Figure 2: Free energy (top) and PMF (bottom) estimation from  $1 \mu\text{s}$  OPES simulations for Chignolin.** We average over four seeds. Green dotted lines indicate the reference value, and blue lines refer to free energy difference during the OPES simulations. Solid lines refer to the mean, and shaded areas are the standard deviation. DeepTICA shows negative values beyond -1 in PMF, even normalized to the DESRES trajectory, falls short of accurately capturing the reference PMF.

## 4 EXPERIMENT RESULTS

**Evaluation setup.** We consider three fast-folding protein in explicit water solvent from [Lindorff-Larsen et al. \(2011\)](#); Chignolin, Trp-cage, and BBA. For more detail on protein data, refer to Section A. We quantitatively evaluate MLCVs with two downstream tasks that require encoding the slow degree of freedom: (i) free energy difference estimation, and (ii) transition path sampling. We use on-the-fly probability enhanced simulation ([Invernizzi & Parrinello, 2020](#), OPES) and CV-steered MD simulation ([Izrailev et al., 1999](#); [Fiorin et al., 2013b](#), SMD) for each task, respectively. Furthermore, we extensively investigate the interpretability of CVs with respect to input descriptors with the sensitivity analysis, and analyze meta-stable state discrimination with secondary structures known to be present in the folded states following [Fu et al. \(2024\)](#).

**Baselines.** We compare our method against self-supervised CV learning methods: DeepTICA ([Bonati et al., 2021](#)), time-lagged autoencoder ([Wehmeyer & Noé, 2018](#), TAE), and variational dynamics encoder ([Hernández et al., 2018](#), VDE). Since protein types and simulation configuration vary significantly by methods and lack systematic comparison, we train from scratch on identical data and time-lag with baselines using the `mlcolvar` package ([Bonati et al., 2023](#)). We use pairwise  $C_\alpha$  distances for inputs to ensure rotation and translation invariance following prior works ([Trizio & Parrinello, 2021](#); [Bonati et al., 2021](#)), and fix CVs dimensionality to one. All MLCVs are normalized to the range  $[-1, 1]$  on the full DESRES trajectory after training for simplicity and visibility, with the sign assigning the folded state to one. For more detail on baselines, refer to Section B.

### 4.1 FREE ENERGY DIFFERENCE ESTIMATION

We first quantify whether MLCVs encode the slow degree of freedom by estimating the free energy difference  $\Delta F$ , with on-the-fly probability enhanced simulations in explicit water solvent.

**On-the-fly probability enhanced simulations.** We run four independent  $1 \mu\text{s}$  on-the-fly probability enhanced sampling ([Invernizzi & Parrinello, 2020](#), OPES) simulations initialized from the folded state. OPES iteratively reconstructs the target probability along the CVs at a pre-defined interval, adding bias that continuously drives transitions between the folded and unfolded states. This enables the estimation of the folding free-energy difference and the potential of mean force (PMF). For more details on the OPES simulations, please refer to Section B.

**Evaluation criteria.** Following [Yang et al. \(2024\)](#), we measure (i) the convergence of the estimated reaction free energy of folding ( $\Delta F$ ), and (ii) the quality of the potential of mean force (PMF). We compute the two meta-stable state basins, folded and unfolded states, by dividing the CV range in half as in prior work. The reference values for each protein are computed from MLCVs of the full DESRES trajectory with the multi-state Bennett acceptance ratio analysis ([Shirts & Chodera,](#)

**Table 2: Quantitative results of steered molecular dynamics on three fast-folding proteins in explicit water solvent.** RMSD and THP are averaged over paths obtained from 16 SMD simulations, while max energy ( $E_{TS}$ ) is averaged over paths hitting the target meta-stable state.  $k$  is the force constant, which is a scaling factor of the harmonic bias potential used in SMD. Best results are highlighted in **bold** and second in underline. We mark not applicable (N/A) for CVs that fail at state discrimination and trajectories not arriving at the target meta-stable state.

Molecule	Method	$k$	RMSD (↓) Å	THP (↑) %	$E_{TS}$ (↓) kJ/mol
Chignolin	DeepTICA	10000	$2.45 \pm 0.86$	37.5	$-81102.41 \pm 521.27$
	TAE	10000	<u><math>1.95 \pm 0.72</math></u>	<u>43.8</u>	$-81914.87 \pm 114.30$
	VDE	10000	$2.08 \pm 0.56$	<u>43.8</u>	$-82026.62 \pm 77.63$
	BIOEMU-CV	10000	<b><math>1.20 \pm 0.33</math></b>	<b>100.0</b>	<b>-82055.15 ± 98.48</b>
Trp-cage	DeepTICA	20000	$2.37 \pm 0.47$	<b>31.2</b>	$-63611.88 \pm 57.49$
	TAE	20000	$2.75 \pm 0.35$	0.0	N/A
	VDE	N/A	N/A	N/A	N/A
	BIOEMU-CV	20000	<b><math>2.31 \pm 0.52</math></b>	<b>31.2</b>	<b>-63787.51 ± 31.23</b>
BBA	DeepTICA	50000	$2.67 \pm 0.37$	18.8	$-130418.50 \pm 477.68$
	TAE	50000	$4.83 \pm 0.42$	0.0	N/A
	VDE	N/A	N/A	N/A	N/A
	BIOEMU-CV	50000	<b><math>2.05 \pm 0.24</math></b>	<b>93.8</b>	<b>-131315.59 ± 116.23</b>

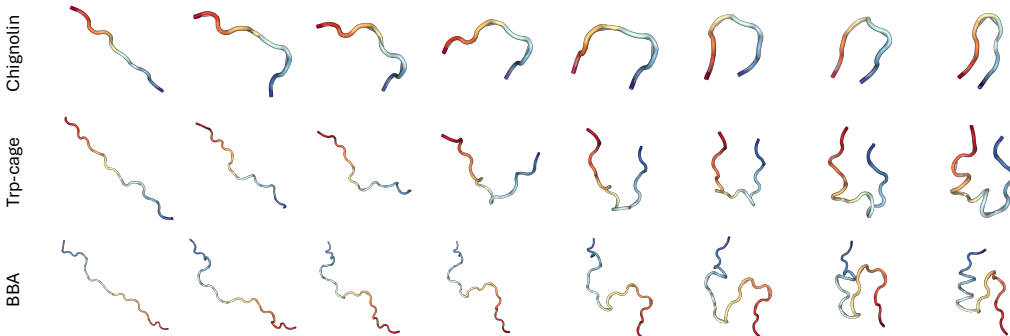


**Figure 3: 3D Visualization of transition paths.** The sampled folding pathways of Chignolin, Trp-cage, and BBA by steered MD with BIOEMU-CV. For simplicity, we visualize the  $C_\alpha$  coordinates.

2008, MBAR). In short, CVs well encoding the slow degree of freedom are expected to have similar distributions between the  $1 \mu s$  OPES simulation and the long naive reference  $\sim 100 \mu s$  DESRES simulation. Note that we exclude results on MLCVs that fail on the basic criterion of discriminating between the folded and unfolded states; see more detail in Section 4.4. Since inadequate CVs produce non-converged biases and misleading PMFs, OPES cannot reliably drive transition, and its PMFs are meaningless. Results are averaged over four runs for Chignolin and three runs for Trp-cage and BBA, with one outlier excluded from the original four following Yang et al. (2024). For more details on evaluation metric and outlier criterion, refer to Section B.

**Results.** In Table 1, we report the reference free energy difference ( $\Delta F_{\text{ref}}$ ), free energy difference averaged over simulations ( $\Delta F$ ), and the potential mean force (PMF) MAE. In Figure 2, we additionally plot the free energy difference throughout the OPES simulations. For the full results, please refer to Section C. In the following, we interpret the results in both quantitative and qualitative aspects. While most MLCVs fairly converge for Chignolin and work for larger proteins, VDE fails to scale to large proteins. Additionally, TAE appears to converge for Trp-cage, but only because it samples exclusively the unfolded state. As shown in Figure 10, the folded state is barely visited resulting convergence at an incorrect  $\Delta F$ , with the wrong sign relative to the reference value. Simi-

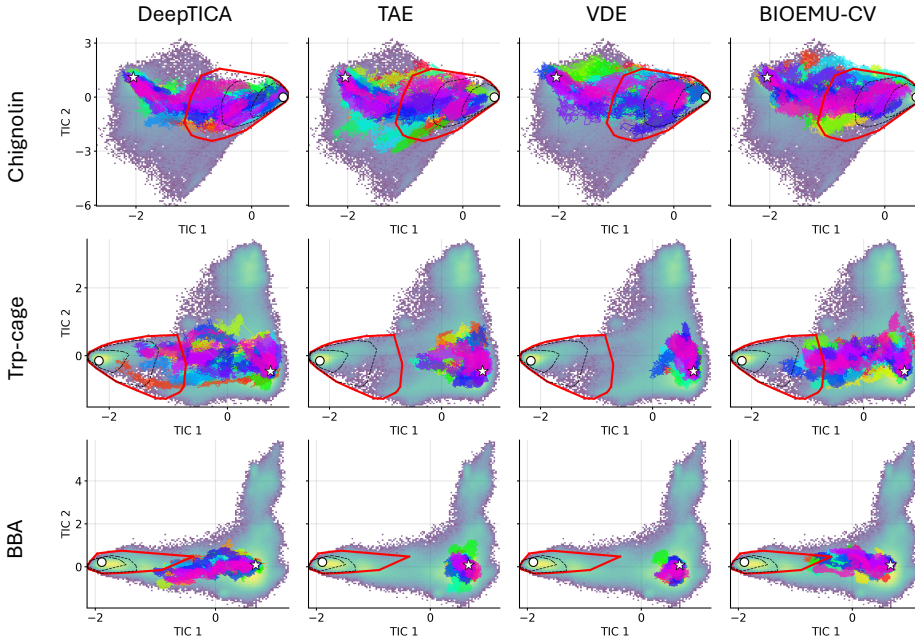


**Figure 4: Transition paths projected onto TICA coordinates, sampled by MLCV steered MD.** The white star and circle each refer to the representative unfolded and folded state, with each paths colored differently. The red convex hull is the folded states defined as RMSD from the representative folded state with cut off 2, 2, and 2.5 Å for Chignolin, Trp-cage, and BBA, respectively.

larly, DeepTICA samples the folded state with high deviation even though the outlier was removed, resulting fluctuation in the PMF. We have clarified more interpretation in detail at Appendix C.

#### 4.2 TRANSITION PATH SAMPLING

We also evaluate the slow degree of freedom in CVs by sampling transition paths of the fast-folding proteins, with CV-steered molecular dynamics simulations in explicit water solvent.

**Steered molecular dynamics.** We sample transition paths with steered molecular dynamics (Izrailev et al., 1999; Fiorin et al., 2013b, SMD). SMD is an enhanced sampling technique that steers the protein conformation towards a pre-defined target state with a time-dependent biasing force. CVs that well encode the slow degree of freedom would produce low-energy transition paths when used with SMD. For each protein, we do 16 NVT simulations for 500 ps using the Langevin Integrator with 1 fs time step. For more detail about SMD, refer to Section B.

**Evaluation criteria.** To evaluate the transition paths from SMD simulations, we first define the target state as the local minimum on the potential energy surface corresponding to the folded state. We then evaluate the transition paths using three metrics from Seong et al. (2025): (i)  $C_\alpha$ -RMSD between the final state of a path and the target state, (ii) the target hit percentage (THP) of sampled paths, and (iii) the transition state energy ( $E_{TS}$ ), i.e., the maximum energy of states of a transition path that hits the target meta-stable state. For THP, a transition path is considered to hit the target meta-stable state if its final state is within 2 Å  $C_\alpha$ -RMSD from the target state, regarding the state definition in Lindorff-Larsen et al. (2011). Again, for the transition path sampling task, any MLCVs that failed to discriminate between the folded and unfolded states of the protein were excluded.

**Results.** In Table 2, BIOEMU-CV shows the best results in hitting the target meta-stable states while achieving low transition state energies. Additionally in Figure 3, we visualize the  $C_\alpha$  atoms in the folding process under BIOEMU-CV steered MD for qualitative assessment. For the visualization of baseline CV-steered MD, refer to Section C. In Figure 4, we also visualize the sampled transition paths of three fast-folding proteins from SMD simulations, by projecting them onto time-lagged independent component analysis (Molgedey & Schuster, 1994, TICA) made from the full DESRES

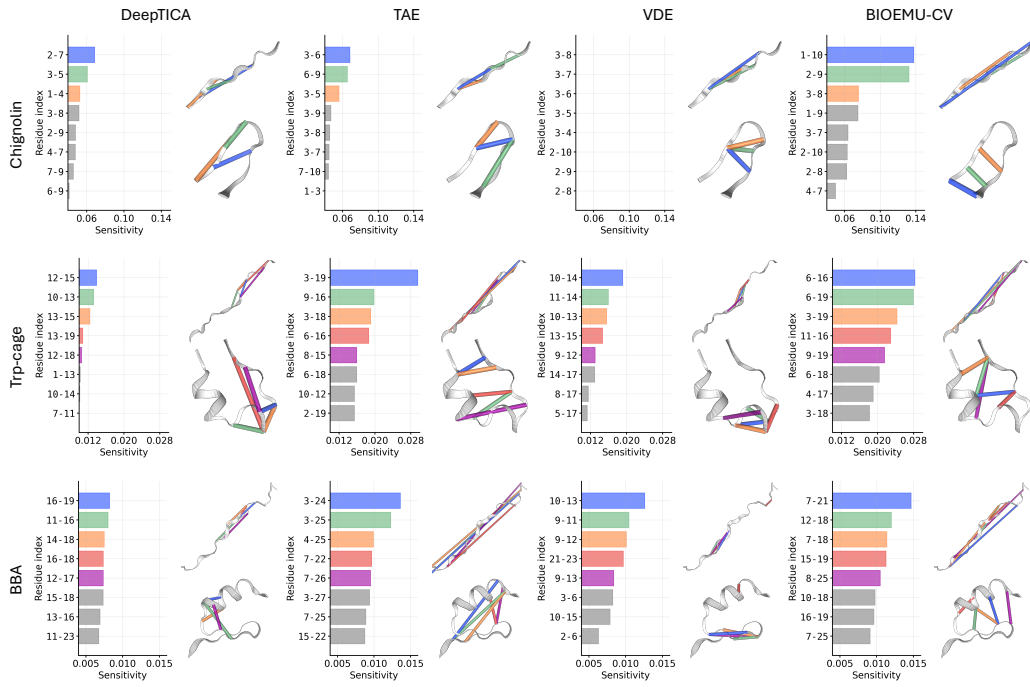


**Figure 5: MLCV sensitivity to  $C_\alpha$ -wise distances.** We plot the top  $C_\alpha$ -wise distances with the highest sensitivity for each MLCV, where the  $x$  and  $y$  axis each denotes the residue index for input distances and the corresponding sensitivity value. For each sensitivity plot, we visualize top sensitive distances in the unfolded and folded state, with colors highlighted in the sensitivity plot.

trajectory. We find that transition paths from our MLCVs show better target reaching and follow the region with a low PMF value defined on two time-lagged independent components.

#### 4.3 INTERPRETABILITY OF CVs

Beyond enhanced sampling tasks, we further assess the physical interpretability of MLCVs.

**Sensitivity analysis.** We evaluate the interpretability of MLCVs by examining how each MLCV changes to their input descriptors, i.e., the sensitivity to the  $C_\alpha$ -wise distance (Bonati et al., 2020; Trizio & Parrinello, 2021). To be specific, we use the `sensitivity_analysis` function from the `mlcolvar` library (Bonati et al., 2023), which computes the sensitivity by the gradients of each MLCV with respect to every input feature. We aggregated the values with the mean of the absolute values, and visualize the top-most sensitive distances in the folded state and unfolded state.

**Results.** As shown in Figure 5, BIOEMU-CV consistently assigns high sensitivity on distances that strongly discriminate the folded and unfolded state, typically long-range contacts spanning the secondary structure for folding. For example in Chignolin, BIOEMU-CV is most sensitive to the distance TYP1–TYR10 and also sensitive to ASP3–TRY8, where a hydrogen bond is observed at folding (Yang et al., 2024). In contrast, DeepTICA and VDE often emphasize distances that provide weaker structural discrimination, e.g., DeepTICA is sensitive to the distances of ASP3–GLU5 and TYR1–PRO4 which does not differ much between the folded and unfolded state. Overall, these results indicate that BIOEMU-CV not only captures the slow dynamical modes required for enhanced sampling, but also learn physically meaningful structural relationships.

#### 4.4 META-STABLE STATE DISCRIMINATION ANALYSIS

Finally, we extensively analyze whether MLCVs clearly discriminate folded and unfolded states, following the criteria of Fu et al. (2024). To be specific, we test whether the folded and unfolded state ensemble occupy distinct ranges of MLCVs and report their distribution statistics across proteins.

**Table 3: State discrimination analysis of MLCVs.** We report the average MLCVs for the folded and unfolded states obtained from the full DESRES trajectory. VDE fails to separate the folded and unfolded states on Trp-cage and BBA, both showing positive ranges.

Method	Chignolin		Trp-cage		BBA	
	Folded	Unfolded	Folded	Unfolded	Folded	Unfolded
DeepTICA	$0.85 \pm 0.06$	$-0.49 \pm 0.11$	$0.70 \pm 0.12$	$-0.74 \pm 0.01$	$0.75 \pm 0.07$	$-0.51 \pm 0.05$
TAE	$0.78 \pm 0.07$	$-0.82 \pm 0.13$	$0.94 \pm 0.03$	$-0.95 \pm 0.02$	$0.40 \pm 0.08$	$-0.90 \pm 0.05$
VDE	$0.84 \pm 0.07$	$-0.74 \pm 0.13$	$1.00 \pm 0.00$	$0.87 \pm 0.13$	$1.00 \pm 0.00$	$1.00 \pm 0.00$
BIOEMU-CV	$0.82 \pm 0.06$	$-0.94 \pm 0.05$	$0.96 \pm 0.03$	$-0.90 \pm 0.03$	$0.94 \pm 0.04$	$-0.93 \pm 0.05$

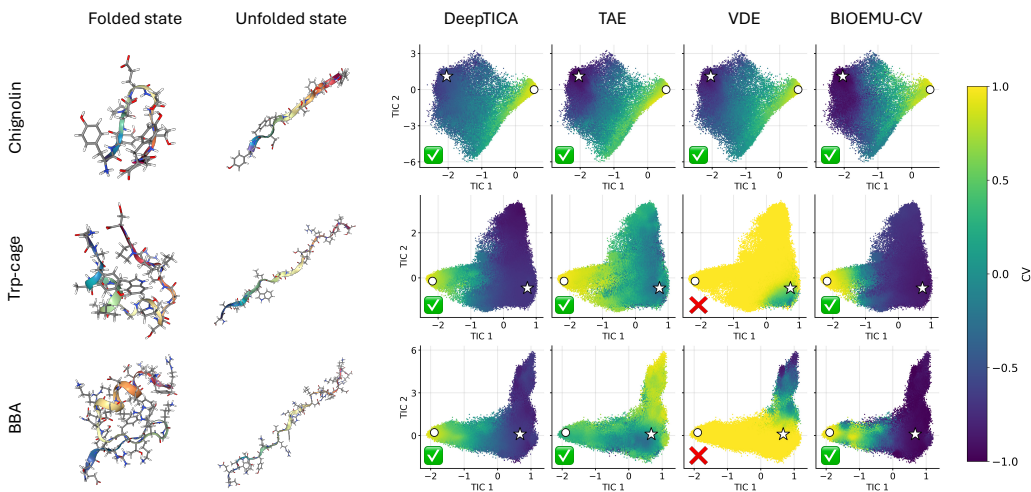


**Figure 6: (Left)** Visualizations of the folded and unfolded states for three protein. **(Right)** TICA projections of the full DESRES trajectory, colored by each MLCVs. The folded and unfolded states are marked by a white circle and a white star, respectively. All MLCVs are normalized to the range  $[-1, 1]$ , with signs flipped such that folded state corresponds to  $+1$  for consistency and visibility. As the protein size increases, prior methods struggle with state discrimination, for instance, VDE.

In case of Chignolin, we cross-validate against standard descriptors, e.g., the committor function and native hydrogen bond numbers. We also probe sensitivity to structural motifs by analyzing the secondary structure elements involved in the folded state, e.g.,  $\alpha$ -helix and  $\beta$ -sheet.

**Meta-stable state discrimination.** First, we verify whether the CVs truly distinguish the folded and unfolded states of proteins. In Figure 6, we color each TICA coordinates with its MLCVs. We use a time lag of  $\tau = 1000$  for BBA and  $\tau = 10$  otherwise for TICA plots. While most methods distinguish the folded and unfolded states, prior works tend to fail at BBA. In Table 3, we report the average MLCVs for the folded and unfolded states gathered from the full DESRES trajectory. Noticeably, VDE shows similar values for Trp-cage and BBA. We plot the detailed distribution of MLCVs for the folded and unfolded states in Section C, where VDE fails at meta-stable state discrimination showing almost identical results between MLCVs of the folded and unfolded states.

**Chignolin analysis.** We also analyze CVs for Chignolin with well-known descriptors, the committor function. The committor function provides a quantitative measure of progress along the folding pathway on a scale from  $[0, 1]$ . We use the committor function from Kang et al. (2024), estimated in a data-driven manner. In Table 4, we report the Pearson correlation between the committor function and MLCVs. DeepTICA shows relatively weak correlation with the committor values, whereas

**Table 4: Pearson correlation** between MLCVs and the Chignolin committor function.

Method	Pearson corr.
DeepTICA	0.682
TAE	0.744
VDE	0.778
BIOEMU-CV	0.748

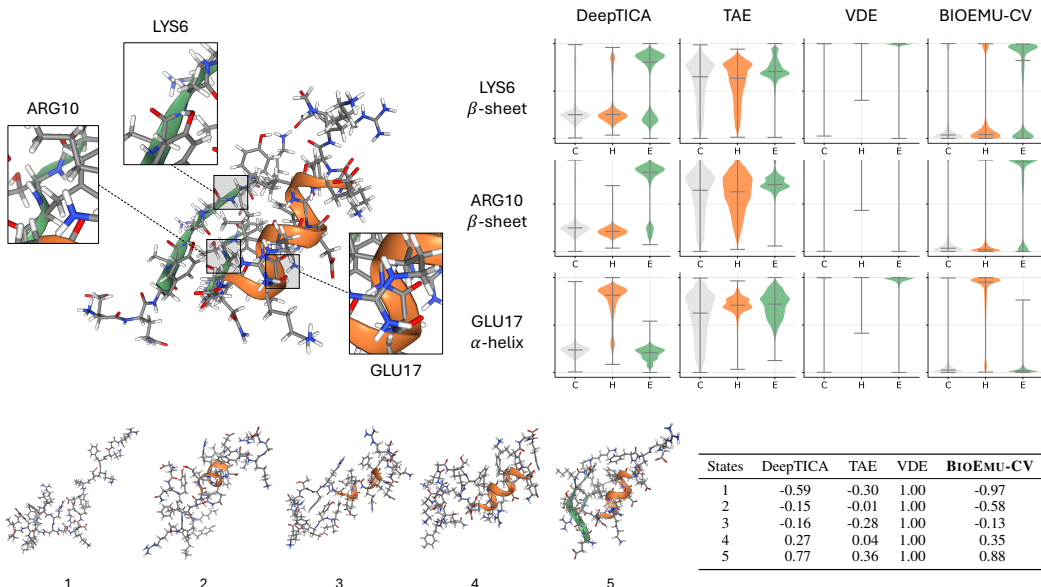


**Figure 7: Secondary structure analysis on BBA.** **(Top)** Folded-state visualization of the BBA protein, with  $\alpha$ -helix and  $\beta$ -sheet highlighted in orange and green, respectively. We also plot the MLCVs distribution for the residues included in the secondary structures, for residues showing specific secondary structures in the folded state. C, H, and E each correspond to coil (irregular elements),  $\alpha$ -helix, and  $\beta$ -sheet secondary structures. TAE and VDE fails to assigns distinct values to helix and sheet structures. **(Bottom)** Visualizations and MLCVs on states in the DESRES trajectory having partial secondary structures. Residues are colored according to the DSSP value. DeepTICA and our MLCVs align with the secondary structures.

other methods demonstrate stronger alignment. For more details on Chignolin descriptors, refer to Section B.

**Secondary structure analysis.** Finally, we analyze the correlation between CVs and the secondary structure of proteins. As seen in Table 5, secondary structures are mostly observed in the folded state clearly distinguished from the unfolded states (Lindorff-Larsen et al., 2011), therefore CVs should capture their presence to describe the folding dynamics (Ahalawat & Mondal, 2018).

We compute the residue-level secondary structure using the *dictionary of secondary structures in proteins* (Kabsch & Sander, 1983; McGibbon et al., 2015, DSSP), which classifies structures based on hydrogen-bond patterns. In Figure 7, we plot the MLCV distribution against the known secondary structures in BBA. While the folded states of BBA contain one  $\alpha$ -helix and two  $\beta$ -sheets (Lindorff-Larsen et al., 2011), TAE and VDE encode nearly identical CVs regardless of the secondary structures in contrast to DeepTICA and BIOEMU-CV successfully separating them.

## 5 CONCLUSION

We present BIOEMU-CV, a lightweight framework that learns collective variables (CVs) from time-lagged conditioning signals on a frozen BioEmu foundation model. Given the current structure, we derive a low-dimensional CV and inject it into BioEmu’s single representation; where only this conditioning path is trained with a denoising score-matching objective, leaving the backbone untouched. We systematically evaluate MLCVs on three fast-folding proteins with two downstream tasks, estimating free energy differences with OPES simulations

**Table 5: Average fraction of residues forming the secondary structure in unfolded states.** Unfolded refers to the fraction of residues regardless of type.

Protein	$\alpha$ -helix	$\beta$ -sheet	Unfolded
Chignolin	0.00	0.00	0.00
Trp-cage	0.02	0.01	0.03
BBA	0.06	0.04	0.08

and transition path sampling with CV-steered MD. Our experiments that BIOEMU-CV successfully identifies important macroscopic movements related to the slow degree of freedom, along with qualitative evaluation on state discrimination.

#### ETHICS STATEMENT

Our work introduces a method to accelerate the study of protein dynamics using the generative model. This work aims to advance scientific understanding of bimolecular mechanisms for disease analysis and drug discovery. We believe the potential for the misuse of this research is low.

#### REPRODUCIBILITY STATEMENT

All protein trajectory data used in this study is publicly available from the D. E. Shaw Research (DESRES) database. The detailed description of the dataset can be found in [Lindorff-Larsen et al. \(2011\)](#). We provided brief explanation of the dataset in Section A.2. Implementation details for our method and all baselines, including model and training hyperparameters, are specified in Section B.2. Furthermore, the experimental setups for our downstream evaluation tasks are provided in the appendix; Section B.3 contains the configurations for the on-the-fly probability enhanced sampling (OPES) simulations, and Section B.4 outlines the setup for the steered molecular dynamics (SMD) simulations. For complete reproduction, we provide our [code](#).

#### THE USE OF LARGE LANGUAGE MODELS (LLMs)

LLMs were only used to aid and polish writing, and has not played a significant role in research ideation and/or writing.

#### ACKNOWLEDGMENTS

Use unnumbered third level headings for the acknowledgments. All acknowledgments, including those to funding agencies, go at the end of the paper.

#### REFERENCES

- Robert Abel, Lingle Wang, Edward D Harder, BJ Berne, and Richard A Friesner. Advancing drug discovery through enhanced free energy calculations. *Accounts of chemical research*, 50(7):1625–1632, 2017. [1](#)
- Mark James Abraham, Teemu Murtola, Roland Schulz, Szilárd Páll, Jeremy C Smith, Berk Hess, and Erik Lindahl. Gromacs: High performance molecular simulations through multi-level parallelism from laptops to supercomputers. *SoftwareX*, 1:19–25, 2015. [19](#)
- Navjeet Ahalawat and Jagannath Mondal. Assessment and optimization of collective variables for protein conformational landscape: Gb1  $\beta$ -hairpin as a case study. *The Journal of chemical physics*, 149(9), 2018. [10](#)
- Alessandro Barducci, Giovanni Bussi, and Michele Parrinello. Well-tempered metadynamics: a smoothly converging and tunable free-energy method. *Physical review letters*, 100(2):020603, 2008. [2](#)
- Alessandro Barducci, Massimiliano Bonomi, and Michele Parrinello. Metadynamics. *Wiley Interdisciplinary Reviews: Computational Molecular Science*, 1(5):826–843, 2011. [1, 2](#)
- Bipasha Barua, Jasper C Lin, Victoria D Williams, Phillip Kummler, Jonathan W Neidigh, and Niels H Andersen. The trp-cage: optimizing the stability of a globular miniprotein. *Protein Engineering, Design & Selection*, 21(3):171–185, 2008. [16](#)
- Robert B Best, Xiao Zhu, Jihyun Shim, Pedro EM Lopes, Jeetain Mittal, Michael Feig, and Alexander D MacKerell Jr. Optimization of the additive charmm all-atom protein force field targeting improved sampling of the backbone  $\phi$ ,  $\psi$  and side-chain  $\chi_1$  and  $\chi_2$  dihedral angles. *Journal of chemical theory and computation*, 8(9):3257–3273, 2012. [20](#)

- Luigi Bonati, Valerio Rizzi, and Michele Parrinello. Data-driven collective variables for enhanced sampling. *The journal of physical chemistry letters*, 11(8):2998–3004, 2020. [2](#), [8](#)
- Luigi Bonati, GiovanniMaria Piccini, and Michele Parrinello. Deep learning the slow modes for rare events sampling. *Proceedings of the National Academy of Sciences*, 118(44):e2113533118, 2021. [2](#), [3](#), [5](#), [18](#)
- Luigi Bonati, Enrico Trizio, Andrea Rizzi, and Michele Parrinello. A unified framework for machine learning collective variables for enhanced sampling simulations: mlcolvar. *The Journal of Chemical Physics*, 159(1), 2023. [2](#), [5](#), [8](#), [18](#), [26](#)
- Giovanni Bussi and Michele Parrinello. Accurate sampling using langevin dynamics. *Physical Review E—Statistical, Nonlinear, and Soft Matter Physics*, 75(5):056707, 2007. [2](#)
- Giovanni Bussi, Davide Donadio, and Michele Parrinello. Canonical sampling through velocity rescaling. *The Journal of chemical physics*, 126(1), 2007. [19](#)
- Marco De Vivo, Matteo Masetti, Giovanni Bottegoni, and Andrea Cavalli. Role of molecular dynamics and related methods in drug discovery. *Journal of medicinal chemistry*, 59(9):4035–4061, 2016. [1](#)
- Peter Eastman, Jason Swails, John D Chodera, Robert T McGibbon, Yutong Zhao, Kyle A Beauchamp, Lee-Ping Wang, Andrew C Simmonett, Matthew P Harrigan, Chaya D Stern, et al. Openmm 7: Rapid development of high performance algorithms for molecular dynamics. *PLoS computational biology*, 13(7):e1005659, 2017. [4](#)
- Peter Eastman, Raimondas Galvelis, Raúl P Peláez, Charles RA Abreu, Stephen E Farr, Emilio Gallicchio, Anton Gorenko, Michael M Henry, Frank Hu, Jing Huang, et al. Openmm 8: molecular dynamics simulation with machine learning potentials. *The Journal of Physical Chemistry B*, 128(1):109–116, 2023. [20](#), [26](#)
- Paul P Ewald. Die berechnung optischer und elektrostatischer gitterpotentiale. *Annalen der physik*, 369(3):253–287, 1921. [20](#)
- Giacomo Fiorin, Jérôme Hénin, and Axel Kohlmeyer. Collective variables module reference manual for lammps. *Albuquerque: Sandia National Laboratories*, 2013a. [20](#)
- Giacomo Fiorin, Michael L Klein, and Jérôme Hénin. Using collective variables to drive molecular dynamics simulations. *Molecular Physics*, 111(22-23):3345–3362, 2013b. [5](#), [7](#), [20](#)
- Haohao Fu, Hengwei Bian, Xueguang Shao, and Wensheng Cai. Collective variable-based enhanced sampling: From human learning to machine learning. *The journal of physical chemistry letters*, 15(6):1774–1783, 2024. [3](#), [5](#), [8](#)
- Donald Hamelberg, John Mongan, and J Andrew McCammon. Accelerated molecular dynamics: a promising and efficient simulation method for biomolecules. *The Journal of chemical physics*, 120(24):11919–11929, 2004. [1](#)
- Jérôme Hénin, Tony Lelièvre, Michael R Shirts, Omar Valsson, and Lucie Delemonette. Enhanced sampling methods for molecular dynamics simulations. *arXiv preprint arXiv:2202.04164*, 2022. [1](#)
- Carlos X Hernández, Hannah K Wayment-Steele, Mohammad M Sultan, Brooke E Husic, and Vijay S Pande. Variational encoding of complex dynamics. *Physical Review E*, 97(6):062412, 2018. [2](#), [3](#), [4](#), [5](#), [18](#)
- Berk Hess, Henk Bekker, Herman JC Berendsen, and Johannes GEM Fraaije. Lincs: A linear constraint solver for molecular simulations. *Journal of computational chemistry*, 18(12):1463–1472, 1997. [19](#)
- Roger Williams Hockney, SP Goel, and JW Eastwood. Quiet high-resolution computer models of a plasma. *Journal of Computational Physics*, 14(2):148–158, 1974. [19](#)

- Moritz Hoffmann, Martin Konrad Scherer, Tim Hempel, Andreas Mardt, Brian de Silva, Brooke Elena Husic, Stefan Klus, Hao Wu, J Nathan Kutz, Steven Brunton, and Frank Noé. Deeptime: a python library for machine learning dynamical models from time series data. *Machine Learning: Science and Technology*, 2021. [24](#)
- Lars Holdijk, Yuanqi Du, Ferry Hooft, Priyank Jaini, Berend Ensing, and Max Welling. Stochastic optimal control for collective variable free sampling of molecular transition paths. *Advances in Neural Information Processing Systems*, 36:79540–79556, 2023. [26](#)
- Shinya Honda, Toshihiko Akiba, Yusuke S Kato, Yoshito Sawada, Masakazu Sekijima, Miyuki Ishimura, Ayako Ooishi, Hideki Watanabe, Takayuki Odahara, and Kazuaki Harata. Crystal structure of a ten-amino acid protein. *Journal of the American Chemical Society*, 130(46):15327–15331, 2008. [16](#)
- Koji Hukushima and Koji Nemoto. Exchange monte carlo method and application to spin glass simulations. *Journal of the Physical Society of Japan*, 65(6):1604–1608, 1996. [2](#)
- Michele Invernizzi and Michele Parrinello. Rethinking metadynamics: from bias potentials to probability distributions. *The journal of physical chemistry letters*, 11(7):2731–2736, 2020. [2](#), [5](#)
- Sergei Izrailev, Sergey Stepaniants, Barry Isralewitz, Dorina Kosztin, Hui Lu, Ferenc Molnar, Willy Wriggers, and Klaus Schulten. Steered molecular dynamics. In *Computational Molecular Dynamics: Challenges, Methods, Ideas: Proceedings of the 2nd International Symposium on Algorithms for Macromolecular Modelling, Berlin, May 21–24, 1997*, pp. 39–65. Springer, 1999. [5](#), [7](#), [20](#)
- William L Jorgensen, Jayaraman Chandrasekhar, Jeffry D Madura, Roger W Impey, and Michael L Klein. Comparison of simple potential functions for simulating liquid water. *The Journal of chemical physics*, 79(2):926–935, 1983. [20](#)
- John Jumper, Richard Evans, Alexander Pritzel, Tim Green, Michael Figurnov, Olaf Ronneberger, Kathryn Tunyasuvunakool, Russ Bates, Augustin Žídek, Anna Potapenko, et al. Highly accurate protein structure prediction with alphafold. *nature*, 596(7873):583–589, 2021. [3](#), [4](#)
- Wolfgang Kabsch. A solution for the best rotation to relate two sets of vectors. *Foundations of Crystallography*, 32(5):922–923, 1976. [26](#)
- Wolfgang Kabsch and Christian Sander. Dictionary of protein secondary structure: pattern recognition of hydrogen-bonded and geometrical features. *Biopolymers: Original Research on Biomolecules*, 22(12):2577–2637, 1983. [10](#), [18](#)
- Peilin Kang, Enrico Trizio, and Michele Parrinello. Computing the committor with the committor to study the transition state ensemble. *Nature Computational Science*, 4(6):451–460, 2024. [9](#), [17](#)
- Diederik P Kingma and Max Welling. Auto-encoding variational bayes. *International conference on Learning representations*, 2014. [3](#)
- Leon Klein and Frank Noé. Transferable boltzmann generators. In *The Thirty-eighth Annual Conference on Neural Information Processing Systems*. PMLR, 2024. [26](#)
- Sarah Lewis, Tim Hempel, José Jiménez-Luna, Michael Gastegger, Yu Xie, Andrew YK Foong, Victor García Satorras, Osama Abdin, Bastiaan S Veeling, Iryna Zaporozhets, et al. Scalable emulation of protein equilibrium ensembles with generative deep learning. *Science*, 389(6761):eadv9817, 2025. [2](#), [3](#), [16](#)
- Kresten Lindorff-Larsen, Stefano Piana, Ron O Dror, and David E Shaw. How fast-folding proteins fold. *Science*, 334(6055):517–520, 2011. [5](#), [7](#), [10](#), [11](#), [16](#), [18](#), [19](#)
- Alex D MacKerell Jr, Donald Bashford, MLDR Bellott, Roland Leslie Dunbrack Jr, Jeffrey D Evanseck, Martin J Field, Stefan Fischer, Jiali Gao, Houyang Guo, Sookhee Ha, et al. All-atom empirical potential for molecular modeling and dynamics studies of proteins. *The journal of physical chemistry B*, 102(18):3586–3616, 1998. [19](#)

- Robert T McGibbon and Vijay S Pande. Variational cross-validation of slow dynamical modes in molecular kinetics. *The Journal of chemical physics*, 142(12), 2015. [24](#)
- Robert T McGibbon, Kyle A Beauchamp, Matthew P Harrigan, Christoph Klein, Jason M Swails, Carlos X Hernández, Christian R Schwantes, Lee-Ping Wang, Thomas J Lane, and Vijay S Pande. Mdtraj: a modern open library for the analysis of molecular dynamics trajectories. *Biophysical journal*, 109(8):1528–1532, 2015. [10](#), [18](#)
- Lutz Molgedey and Heinz Georg Schuster. Separation of a mixture of independent signals using time delayed correlations. *Physical review letters*, 72(23):3634, 1994. [3](#), [7](#), [16](#)
- Chong Mou, Xintao Wang, Liangbin Xie, Yanze Wu, Jian Zhang, Zhongang Qi, and Ying Shan. T2i-adapter: Learning adapters to dig out more controllable ability for text-to-image diffusion models. In *Proceedings of the AAAI conference on artificial intelligence*, volume 38, pp. 4296–4304, 2024. [2](#), [3](#), [4](#)
- Yusuke Naritomi and Sotaro Fuchigami. Slow dynamics in protein fluctuations revealed by time-structure based independent component analysis: the case of domain motions. *The Journal of chemical physics*, 134(6), 2011. [16](#)
- Frank Noé and Cecilia Clementi. Kinetic distance and kinetic maps from molecular dynamics simulation. *Journal of chemical theory and computation*, 11(10):5002–5011, 2015. [24](#)
- Frank Noé and Cecilia Clementi. Collective variables for the study of long-time kinetics from molecular trajectories: theory and methods. *Current opinion in structural biology*, 43:141–147, 2017. [2](#)
- Frank Noé and Feliks Nuske. A variational approach to modeling slow processes in stochastic dynamical systems. *Multiscale Modeling & Simulation*, 11(2):635–655, 2013. [24](#)
- Stefano Piana and Alessandro Laio. A bias-exchange approach to protein folding. *The journal of physical chemistry B*, 111(17):4553–4559, 2007. [2](#)
- Stefano Piana, Kresten Lindorff-Larsen, and David E Shaw. How robust are protein folding simulations with respect to force field parameterization? *Biophysical journal*, 100(9):L47–L49, 2011. [19](#)
- Stefano Piana, Kresten Lindorff-Larsen, and David E Shaw. Protein folding kinetics and thermodynamics from atomistic simulation. *Proceedings of the National Academy of Sciences*, 109(44):17845–17850, 2012. [1](#)
- Fabio Pietrucci and Alessandro Laio. A collective variable for the efficient exploration of protein beta-sheet structures: application to sh3 and gb1. *Journal of Chemical Theory and Computation*, 5(9):2197–2201, 2009. [2](#)
- David E Rumelhart, Geoffrey E Hinton, Ronald J Williams, et al. Learning internal representations by error propagation, 1985. [3](#)
- Catherine A Sarisky and Stephen L Mayo. The  $\beta\beta\alpha$  fold: explorations in sequence space. *Journal of molecular biology*, 307(5):1411–1418, 2001. [16](#)
- Martin K Scherer, Benjamin Trendelkamp-Schroer, Fabian Paul, Guillermo Pérez-Hernández, Moritz Hoffmann, Nuria Plattner, Christoph Wehmeyer, Jan-Hendrik Prinz, and Frank Noé. Pyemma 2: A software package for estimation, validation, and analysis of markov models. *Journal of chemical theory and computation*, 11(11):5525–5542, 2015. [16](#)
- Kiyoung Seong, Seonghyun Park, Seonghwan Kim, Woo Youn Kim, and Sungsoo Ahn. Transition path sampling with improved off-policy training of diffusion path samplers. *arXiv preprint arXiv:2405.19961*, 2025. [7](#), [26](#)
- Michael R Shirts and John D Chodera. Statistically optimal analysis of samples from multiple equilibrium states. *The Journal of chemical physics*, 129(12), 2008. [5](#)

- Yang Song, Jascha Sohl-Dickstein, Diederik P Kingma, Abhishek Kumar, Stefano Ermon, and Ben Poole. Score-based generative modeling through stochastic differential equations. *arXiv preprint arXiv:2011.13456*, 2020. [4](#)
- Evan Walter Clark Spotte-Smith, Ronald L Kam, Daniel Barter, Xiaowei Xie, Tingzheng Hou, Shyam Dwaraknath, Samuel M Blau, and Kristin A Persson. Toward a mechanistic model of solid–electrolyte interphase formation and evolution in lithium-ion batteries. *ACS Energy Letters*, 7(4):1446–1453, 2022. [1](#)
- Yuji Sugita and Yuko Okamoto. Replica-exchange molecular dynamics method for protein folding. *Chemical physics letters*, 314(1-2):141–151, 1999. [1](#)
- Gareth A Tribello, Massimiliano Bonomi, Davide Branduardi, Carlo Camilloni, and Giovanni Bussi. Plumed 2: New feathers for an old bird. *Computer physics communications*, 185(2):604–613, 2014. [19](#)
- Enrico Trizio and Michele Parrinello. From enhanced sampling to reaction profiles. *The Journal of Physical Chemistry Letters*, 12(35):8621–8626, 2021. [2](#), [5](#), [8](#)
- Omar Valsson, Pratyush Tiwary, and Michele Parrinello. Enhancing important fluctuations: Rare events and metadynamics from a conceptual viewpoint. *Annual review of physical chemistry*, 67(1):159–184, 2016. [2](#)
- Gian Marco Visani, William Galvin, Michael Pun, and Armita Nourmohammad. H-packer: Holographic rotationally equivariant convolutional neural network for protein side-chain packing. In *Machine Learning in Computational Biology*, pp. 230–249. PMLR, 2024. [4](#)
- Dedi Wang, Yunrui Qiu, Eric R Beyerle, Xuhui Huang, and Pratyush Tiwary. Information bottleneck approach for markov model construction. *Journal of chemical theory and computation*, 20(12):5352–5367, 2024. [24](#)
- Christoph Wehmeyer and Frank Noé. Time-lagged autoencoders: Deep learning of slow collective variables for molecular kinetics. *The Journal of chemical physics*, 148(24), 2018. [2](#), [3](#), [5](#), [18](#)
- Hao Wu and Frank Noé. Variational approach for learning markov processes from time series data. *Journal of Nonlinear Science*, 30(1):23–66, 2020. [24](#)
- Soojung Yang, Juno Nam, Johannes CB Dietschreit, and Rafael Gómez-Bombarelli. Learning collective variables with synthetic data augmentation through physics-inspired geodesic interpolation. *Journal of Chemical Theory and Computation*, 20(15):6559–6568, 2024. [5](#), [6](#), [8](#), [17](#), [19](#)
- Jason Yim, Brian L Trippe, Valentin De Bortoli, Emile Mathieu, Arnaud Doucet, Regina Barzilay, and Tommi Jaakkola. Se (3) diffusion model with application to protein backbone generation. In *International conference on machine learning*. PMLR, 2021. [4](#)
- Lvmin Zhang, Anyi Rao, and Maneesh Agrawala. Adding conditional control to text-to-image diffusion models. In *Proceedings of the IEEE/CVF international conference on computer vision*, pp. 3836–3847, 2023. [2](#), [3](#), [4](#)

## A DATA DETAILS

### A.1 PROTEIN DATA

Proteins are a sequence of amino acid building blocks, each represented by one letter. Below, we provide statistics on the proteins we used in this work. Protein size ranges from 10 to 35 residues, 166 to 504 atoms. C The PDB ID in the Table 6 refers to the discovered experimental structures in the PDB with the smallest error. In case of Chignolin, it is closest to the NMR structure of CLN025 reported by [Honda et al. \(2008\)](#). Trp-cage corresponds to the K8A mutant of the thermostable Trp-cage variant TC10b in [Barua et al. \(2008\)](#), and BBA, i.e., short for beta-beta-alpha, corresponds to the FDS-EY peptide in [Sarisky & Mayo \(2001\)](#).

Table 6: **Details on three proteins** used in this work, selected among the DESRES fast folding proteins.

Protein	PDB ID	# of Residues	# of Atoms	# of CA pairs	Sequence
Chignolin	CLN025	10	166	45	YYDPETGTWY
Trp-cage	2JOF	20	272	190	DAYAQWLKDHHPPSSGRPPPS
BBA	1FME	28	504	378	LSDEDFAVFGMTRSAFANLPLWXQQHLXKEKGLF

### A.2 DESRES TRAJECTORY DATASET

[Lindorff-Larsen et al. \(2011\)](#) provides twelve fast-folding proteins. Among them, we chose three proteins to test MLCVs. For proteins given with multiple simulations, we sample from the longest length simulation to use as the data. In other words, we use the simulation of length 223  $\mu\text{s}$  for the BBA protein. In Table 7, we denote the simulation time, average folding time, simulation temperature, and the cubic box size of the simulations. Since DESRES simulations are recorded in 0.2 picoseconds intervals and reach millions of frames, we chose to randomly sample 50,000 frames as in [Lewis et al. \(2025\)](#).

Table 7: **Simulation details** of three DESRES fast-folding proteins.

Protein	Simulation time ( $\mu\text{s}$ )	Avg. folding time ( $\mu\text{s}$ )	Temperature (K)	Cubic box ( $\text{\AA}$ )
Chignolin	106	0.6	340	40
Trp-cage	208	14	290	37
BBA	223, 102	2.8	325	47

### A.3 TIME-LAGGED INDEPENDENT COMPONENT ANALYSIS

Time-lagged independent component analysis ([Molgedey & Schuster, 1994](#), TICA) is a linear transformation method commonly used for dimensionality reduction, first used for molecular dynamics in [Naritomi & Fuchigami \(2011\)](#). In short, it maps the given data to the slow process for a given time-lag  $\tau$ , by finding the coordinates of maximal auto correlation between time-lagged data pairs. Therefore, TICA, combined with a long MD trajectory, will likely capture the slow degree of freedom well. In this work, we use the TICA model in pyemma ([Scherer et al., 2015](#)). All TICA plots in the paper, e.g., Figure 4 and Figure 6, are made with the full DESRES trajectory with a log norm applied. We use  $C_\alpha$  pairwise distances for the input descriptors, and apply the switching function to obtain the contact  $s_{ij}$  in the case of Chignolin as follows:

$$s_{ij} = \frac{1 - (r_{ij}/r_0)^n}{1 - (r_{ij}/r_0)^m},$$

where  $r_{ij}$  refers to the distances between  $C_\alpha$  atoms  $i$  and  $j$ ,  $r_0=0.8\text{nm}$ ,  $n = 6$ , and  $m = 12$ . Intuitively, the contacts  $s_{ij}$  are a continuous version of the coordinate numbers.

## B SIMULATION AND EVALUATION DETAILS

### B.1 QUALITATIVE VERIFICATION

**CLN025 descriptors.** CLN025 is known to form several hydrogen bonds at the folded state (Yang et al., 2024). The criteria for hydrogen bonds are (i) the donor-acceptor distance being smaller than  $0.35\text{ nm}$ , and (ii) the angle formed by the donor, acceptor, and hydrogen being bigger than  $110^\circ$ . The donor acceptor atom list is as follows:

1. TYR1 N, TYR10 OT1
2. TYR1 N, TYR10 OXT
3. ASP3 N, TRY8 O
4. THR6 OG1, ASP3 O
5. THR6 N, ASP3 OD1
6. THR6 N, ASP3 OD2
7. GLY7 N, ASP3 O
8. TYR10 N, TYR1 O

**Committor function.** The committer function  $q(x)$  is the probability that a trajectory initiated from a configuration  $x$  reaches the folded state  $B$  before the unfolded state  $A$ . It is the solution to the backward Kolmogorov equation with the boundary conditions  $q(x) = 0$  for  $x \in A$  and  $q(x) = 1$  for  $x \in B$ . We use the committer function from Kang et al. (2024) to evaluate its correlation with MLCVs. In their approach, solving the Kolmogorov equation is reformulated as minimizing a variational functional. To this end, they parameterize the committer function as a neural network and train it using a self-consistent iterative procedure to optimize the functional.

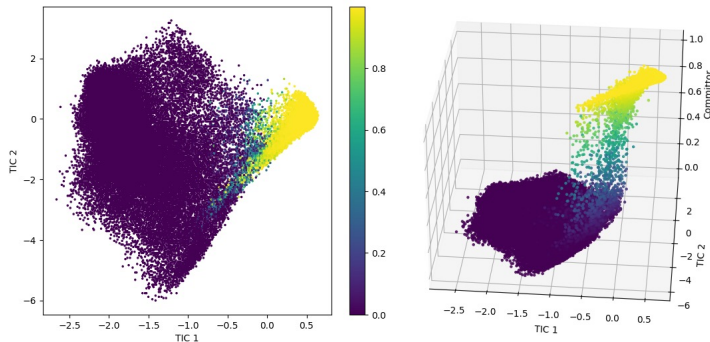


Figure 8: TICA coordinates colored with committer values.

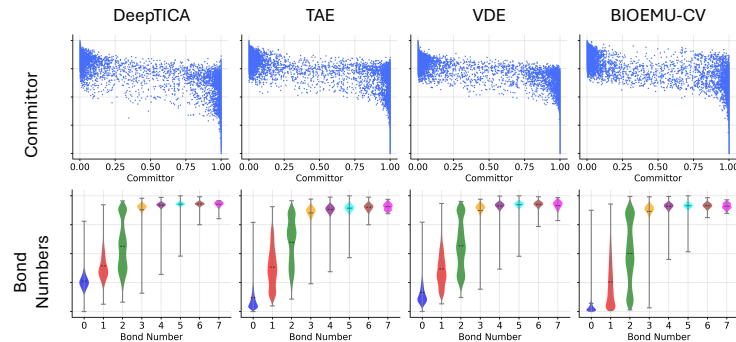


Figure 9: Correlation to known descriptors for Chignolin. (Top) Scatter plot of correlation to the committer function. (Bottom) Violin plot of correlation to the number of hydrogen bonds.

**Secondary structure.** Protein secondary structures are local spatial structures made from the backbone excluding the side chain, key structures observed in the folded states. The two most common structures are the  $\alpha$ -helix and  $\beta$ -sheet shown in Figure 7, i.e., spiral coil-like structure and flattened zig-zag-shaped structure, respectively. Secondary structures are formally defined by the pattern of hydrogen bonds between the hydrogen atoms in the amino part and the oxygen atoms in the carboxyl. In this work, we use the *dictionary of secondary structures proteins* (Kabsch & Sander, 1983, DSSP) for the definition of secondary structures, implemented in the MDtraj library (McGibbon et al., 2015). Note that secondary structures are assigned for each residue, and three or more consecutive residues with the same hydrogen bond are usually considered a full secondary structure. For proteins simulated in Lindorff-Larsen et al. (2011), secondary structures are rarely observed in the unfolded state as stated in Table 5. Additionally, in Table 8, we list the percentage of secondary structures throughout the whole DESRES trajectory for each residue and protein. Three classes of DSSP: C, E, and H each correspond to irregular elements,  $\beta$ -sheets, and  $\alpha$ -helix. While DDSP provides a detailed classification with eight classes, we selected the simplified one for this work.

Table 8: DSSP class percentage of each residue in Chignolin, Trp-cage, and BBA.

DSSP	0	1	2	3	4	5	6	7	8	9
C	100.0	25.5	53.8	99.2	98.6	98.4	98.5	52.7	24.7	100.0
E	0.0	74.5	46.2	0.0	0.2	0.1	0.1	46.3	74.6	0.0
H	0.0	0.0	0.0	0.8	1.2	1.5	1.5	1.0	0.6	0.0
Trp-cage	0	1	2	3	4	5	6	7	8	9
C	100.0	85.7	75.1	70.9	67.1	67.8	72.3	78.2	88.8	97.7
E	0.0	0.3	1.4	1.2	3.0	4.0	2.7	1.3	0.5	0.1
H	0.0	14.0	23.6	27.9	29.8	28.3	25.0	20.5	10.7	2.2
Trp-cage	10	11	12	13	14	15	16	17	18	19
C	83.6	80.9	75.7	80.1	95.6	94.6	100.0	100.0	99.8	100.0
E	1.7	2.1	4.6	2.4	0.6	5.4	0.0	0.0	0.2	0.0
H	14.7	17.0	19.7	17.5	3.8	0.0	0.0	0.0	0.0	0.0
BBA	0	1	2	3	4	5	6	7	8	9
C	100.0	96.4	79.1	75.5	68.1	64.6	70.1	89.2	93.7	73.9
E	0.0	3.0	9.5	10.7	16.0	21.0	23.1	5.1	1.3	20.2
H	0.0	0.6	11.4	13.8	15.9	14.4	6.8	5.6	5.0	5.9
BBA	10	11	12	13	14	15	16	17	18	19
C	70.8	75.5	91.0	94.6	71.6	67.5	67.3	67.3	67.4	67.7
E	23.8	19.4	5.9	3.8	3.0	4.6	4.3	2.9	2.7	2.6
H	5.5	5.1	3.2	1.5	25.4	27.9	28.4	29.8	30.0	29.7
BBA	20	21	22	23	24	25	26	27		
C	61.2	61.5	65.6	71.2	83.6	94.0	98.5	100.0		
E	4.6	5.6	4.1	2.4	4.6	2.3	0.6	0.0		
H	34.2	32.9	30.2	26.4	11.8	3.7	0.9	0.0		

## B.2 BASELINE DETAILS

We test three self-supervised time-lagged MLCV baselines: DeepTICA (Bonati et al., 2021), TAE (Wehmeyer & Noé, 2018), and VDE (Hernández et al., 2018). Since simulation configurations vary in each paper, we retrain all models with the same data using the `mlcolvar` library (Bonati et al., 2023). All models have the following identical configurations. We use a neural network size of [45, 100, 100, 1] with tanh as the activation function, and a dropout of 0.5. We split the dataset into 80% for training and 20% for validation. Models, including ours, were trained for a maximum of 1000 epochs, with early stopping applied with a minimum delta of 0.1 and patience of 50 epochs. Unless mentioned, we follow the basic configuration of the `mlcolvar` (Bonati et al., 2023).

### B.3 OPES SIMULATION DETAILS

**Simulation settings.** OPES simulations for all proteins were performed with GROMACS 2024.3 (Abraham et al., 2015) patched with PLUMED 2.10 (Tribello et al., 2014), on top of Docker containers. Proteins were solvated in a cubic water with the same size as the reference simulation data, and each neutralized using sodium or chloride ions. The protein molecule was parameterized by the CHARMM27 force field (Piana et al., 2011), i.e., CHARMM22 plus CMAP backbone correction, and the modified TIP3P water model compatible with the CHARMM force field (MacKerell Jr et al., 1998), analogously to the reference simulation data (Lindorff-Larsen et al., 2011). Simulations were all performed in the NVT ensemble. Initial states were selected from folded states among the original DESRES trajectory, where the folded state was identified with native contacts and secondary structures. Afterward, the state was equilibrated through short NVT and NPT simulations, each of length 50 and 500 picoseconds, respectively. Temperatures were controlled with the velocity rescaling thermostat (v-rescale) (Bussi et al., 2007). Equations of motion were integrated with a time step of 2 femtoseconds with the leap-frog algorithm (Hockney et al., 1974). Additionally, the LINCS algorithm (Hess et al., 1997) was used to constrain all bonds involving the hydrogen bonds. All simulations were run on a single GPU of RTX 3090 or RTX 4090, with four to nine days depending on the protein size. Approximately 8,000 GPU hours were used for a single evaluation.

**OPES configurations.** We use configurations as in Table 9 for PLUMED, differing only in temperatures. A PACE of 500 steps is applied, i.e., 1 picoseconds. We use the same SIGMA value 0.05 and BARRIER value 30 for all systems. Temperatures are identical to the reference simulation. The first 100 ns are discarded as equilibration time with 50 ns window unit time steps for Figures 2 and 10.

Table 9: **OPES Simulation details** of three DESRES fast-folding proteins.

Protein	PACE	SIGMA	BARRIER (kJ/mol)	Temperature (K)
Chignolin	500	0.05	30	340
Trp-cage (TC10b)	500	0.05	30	290
BBA	500	0.05	30	325

**Evaluation metrics.** We evaluate the learned collective variables (CVs) using two complementary metrics from Yang et al. (2024): the free energy difference  $\Delta F$  and the mean absolute error (MAE) of the potential of mean force (PMF). The free energy difference  $\Delta F$  quantifies the stability gap between the folded and unfolded states. It is computed by integrating the PMF  $A(s)$  for CVs  $s$  over the corresponding metastable basins,

$$\Delta F = -k_B T \log \left( \frac{\int_{\text{folded}} \exp(-A(s)/k_B T) ds}{\int_{\text{unfolded}} \exp(-A(s)/k_B T) ds} \right), \quad (2)$$

where  $k_B$  is the Boltzmann constant and  $T$  is the temperature. A lower  $\Delta F$  error indicates that the CV preserves the free energy difference between metastable states more accurately. For the folded and unfolded basins, we divided the reference CVs range to half and use them for each one.

In addition, we use the mean absolute error (MAE) of the PMF to evaluate the agreement between the biased and reference free-energy landscapes. PMF, The MAE is defined as

$$\text{MAE}(A, A_{\text{ref}}) = \frac{\int |A(s) - A_{\text{ref}}(s)| \mathbb{I}[A_{\text{ref}}(s) < A_{\text{thres}}] ds}{\int \mathbb{I}[A_{\text{ref}}(s) < A_{\text{thres}}] ds}, \quad (3)$$

where  $A(s)$  and  $A_{\text{ref}}(s)$  are the PMFs from enhanced sampling and a long unbiased trajectory, respectively, and  $\mathbb{I}[\cdot]$  is an indicator function restricting the comparison to regions with reference free energy below a threshold  $A_{\text{thres}} = 25$  kJ/mol. This metric captures deviations in both metastable basins and transition regions.

**Outlier simulation exclusion.** As discussed in Yang et al. (2024), enhanced sampling simulations driven by CVs may often get trapped in a local minima, leading to outlier simulation results. To address this issue, we follow the standard practice of computing the metrics after removing a single outlier run. Specifically, among the four simulations, we identify the outlier based on the final free energy difference, i.e., the run whose value deviates the most from the mean, and exclude it. Afterwards, the metrics are re-computed using the remaining three runs.

#### B.4 STEERED MD SIMULATION DETAILS

Steered MD ([Izrailev et al., 1999](#); [Fiorin et al., 2013b](#), SMD) is an enhanced sampling method for sampling transition paths. It drives the state toward the target meta-stable state along the time-dependent reference CV using an additional harmonic potential. This biasing potential of SMD is defined as

$$U(x, t) = \frac{k}{2} \|c(x) - c_t^{\text{ref}}\|^2, \quad c_t^{\text{ref}} = c^{\text{initial}} + \frac{(c^{\text{target}} - c^{\text{initial}})t}{T}, \quad (4)$$

where  $k$  is the force constant,  $x$  the molecular configuration,  $t$  is the current step,  $T$  the total number of steps, and  $c^{\text{initial}}$ ,  $c^{\text{target}}$  are the CV values at the respective meta-stable states. The reference CV starts at the initial CV  $c^{\text{initial}}$  and ends at the target CV  $c^{\text{target}}$  with constant rate  $(c^{\text{target}} - c^{\text{initial}})/T$ . The bias potential  $U(x, t)$  restrains the current state to follow the reference states. To hit the target meta-stable states better, in our experiments, we combine the MLCVs  $f_\theta(x)$  with (Kabsch aligned)  $C_\alpha$ -RMSD CV as  $c(x) = f_\theta(x) - \text{RMSD}(x, x_{\text{target}})$ , following the technique supported in [Fiorin et al. \(2013a\)](#).

We perform SMD simulations with the OpenMM software package ([Eastman et al., 2023](#)) to generate transition pathways. We use the CHARMM36 force field ([Best et al., 2012](#)) for the fast-folding proteins and the modified TIP3P model ([Jorgensen et al., 1983](#)) for water molecules. We handle long-range electrostatics via the Particle Mesh Ewald (PME) method ([Ewald, 1921](#)) with a 0.95 nm cutoff. Constraining all bonds involving hydrogen atoms allow for a 1 fs integration timestep. We run the simulations in the canonical (NVT) ensemble at 340 K. A Langevin integrator with a 1 ps<sup>-1</sup> friction coefficient is used for the 500 ps NVT equilibration. Finally, since the CV depends only on the  $C_\alpha$  atom coordinates, we apply the biasing force,  $-\nabla_x U(x, t)$ , exclusively to them through the OpenMM external force class.

## C ADDITIONAL RESULTS

### C.1 OPES SIMULATION RESULTS

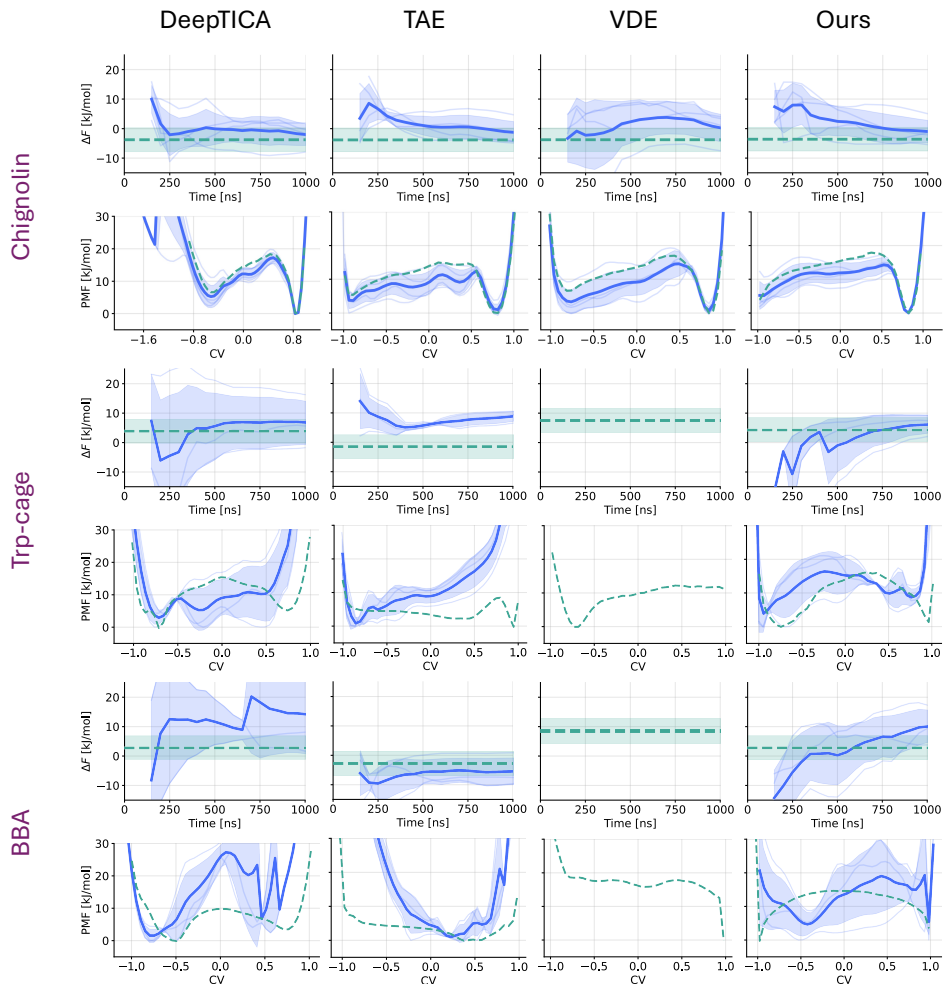


Figure 10: **Free energy difference (top)** and **PMF (bottom)** for three proteins from  $1 \mu s$  OPES simulation. Green dotted lines indicate the reference value computed by CVs along the full DESRES trajectory, while blue lines refer to values computed by CVs from the OPES simulations.

In Figure 10, Chignolin fairly converges while Trp-cage and BBA show relatively big deviations. In the following, we qualitatively evaluate MLCVs for each protein averaged over three simulations.

**Trp-cage.** Although TAE converged with a small deviation, this is due to failing to sample enough folded states. Also, the PMF for the folded state does not align with the reference, especially regarding the folded state region, i.e., the positive range of CVs. This indicates the failure of sampling folded states, which leads to incorrect energy value convergence. Additionally, DeepTICA shows a very low PMF compared to the reference PMF near  $CV \approx 0$ . This indicates that while the unfolded states were sampled properly, the folded states were not sampled enough or CVs identified as the folded states were actually transition states, resulting in a severe mismatch between PMFs.

**BBA.** Once again, although TAE appears to converge closely to the reference value, we can identify that only the folded states are exclusively sampled from the PMF plot. Unfolded states, i.e., CVs being close -1, are not sampled at all, resulting in a convergence to an incorrect value. Furthermore, the reference PMF shows only one distinct local minimum, indicating that the trained CV itself did not properly discriminate between the folded and unfolded states. While one outlier simulation has

been excluded for DeepTICA, the PMF plot shows divergence between simulations near the folded states. This indicates that DeepTICA has failed to sample folded states properly, such as assigning diverse CV values to similar folded states.

## C.2 STATE DISCRIMINATION

In this section, we present the full qualitative results extended from Section 4.4. In Figure 11, we visualize the MLCV value on the z-axis on top of the TICA plane. In Figure 12, we visualize the violin plot of the MLCV of the folded and unfolded state. The states are collected from the full DESRES trajectory, with an RMSD threshold cutoff.

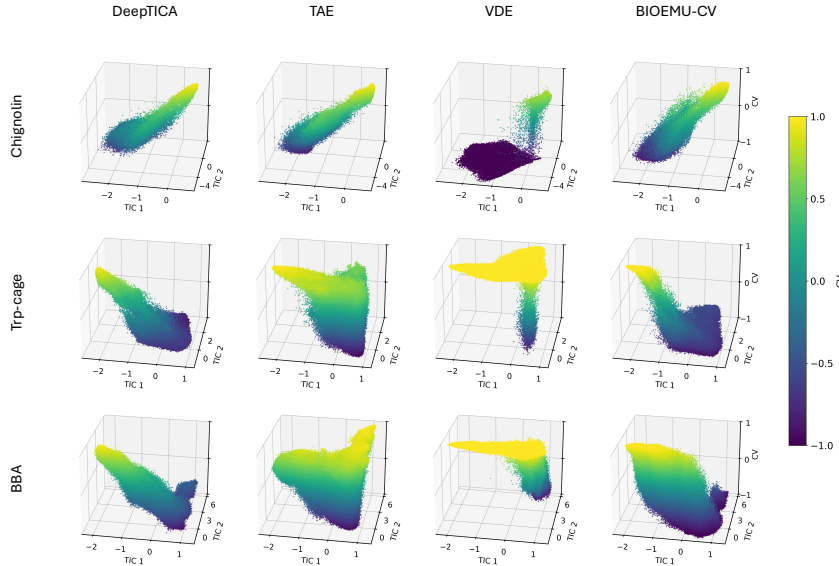


Figure 11: **3D visualization of protein conformations projected to TICA coordinates, with ML-CVs as the z axis.**

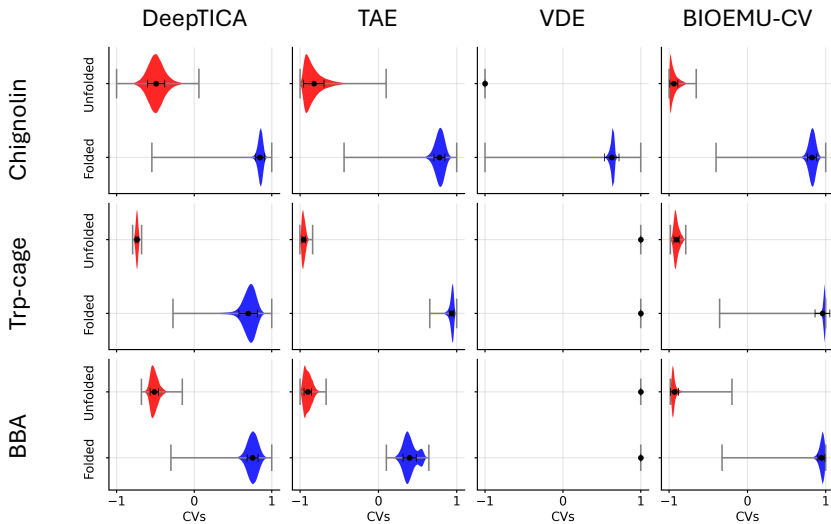
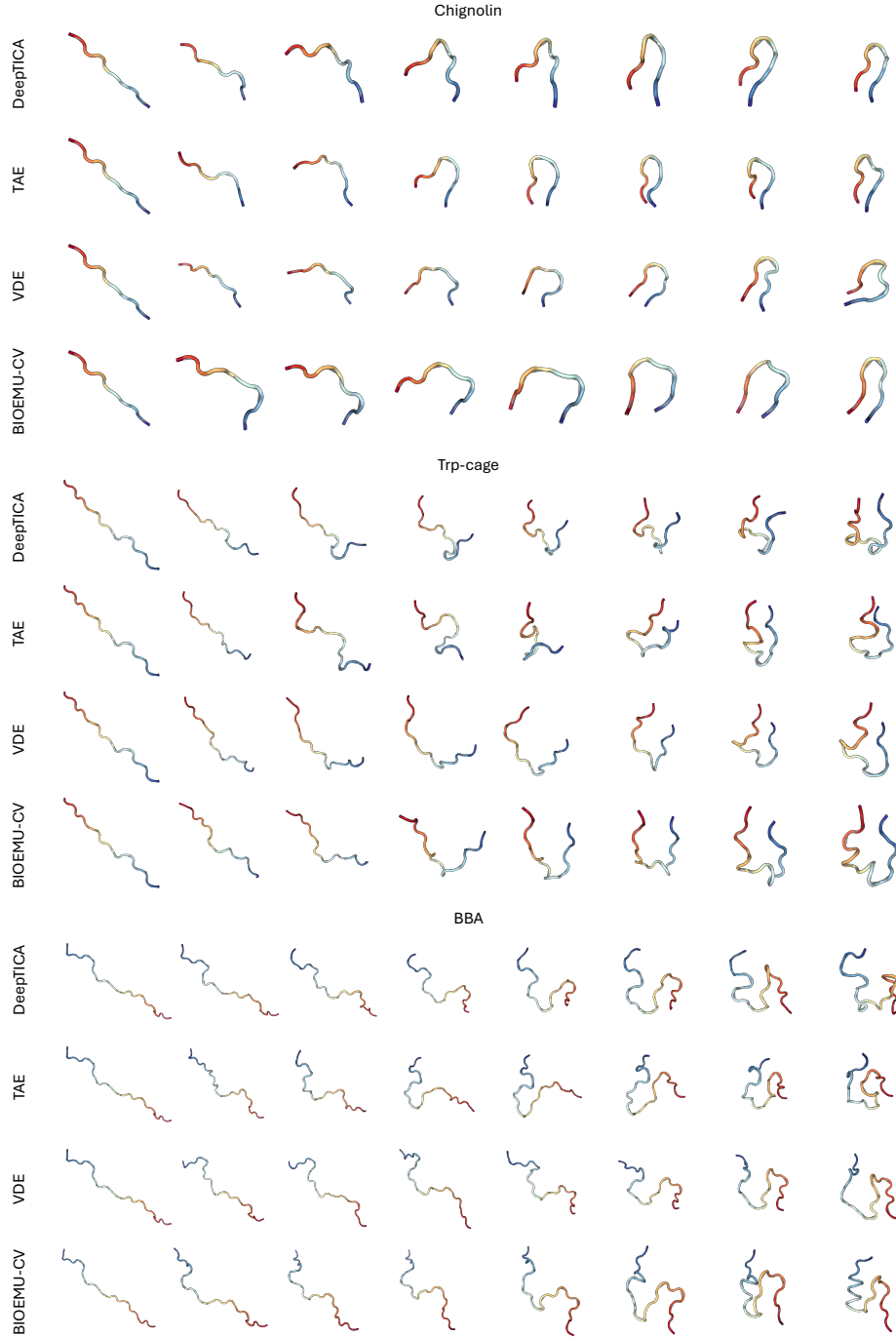


Figure 12: **MLCV distribution of the folded and unfolded states.** Average MLCV of the folded and unfolded state is stated as the black dot, with the standard deviation in black lines.

### C.3 STEERED MD VISUALIZATION

We also visualize  $C_\alpha$  of MLCV-steered MD trajectory for all baselines, following Figure 3. For the folded state visualization in the DESRES data, refer to the one in Figure 6.



**Figure 13: 3D Visualization of MLCV-steered MD paths.** The sampled folding pathways of Chignolin, Trp-cage, and BBA by steered MD with MLCVs from DeepTICA, TAE, VDE, and BIOEMU-CV.

#### C.4 VAMP SCORE

Here, we evaluate the VAMP score (Noé & Nuske, 2013; McGibbon & Pande, 2015; Noé & Clementi, 2015; Wu & Noé, 2020) on MLCVs, where a higher VAMP score indicates preservation of dynamic contents. We use VAMP from `deeptime` library (Hoffmann et al., 2021), with a time-lag of 10 on the DESRES trajectory data. In Table 10, TAE and VDE show a relatively low score for bigger molecules compared to other methods. DeepTICA yields a high score since its training objective is similar to the definition of the VAMP score, and BioEMU-CV shows similar VAMP scores in big molecules. However, VAMP scores should not be simply trusted since highly correlated values could result in high VAMP scores (Noé & Nuske, 2013; Wang et al., 2024).

Table 10: **VAMP scores of MLCVs** for Chignolin, Trp-cage, and BBA. A higher score indicates better preservation of dynamic content.

Method	Chignolin			Trp-cage			BBA		
	VAMP-1	VAMP-2	VAMP-E	VAMP-1	VAMP-2	VAMP-E	VAMP-1	VAMP-2	VAMP-E
DeepTICA	1.9803	1.9611	1.9611	1.9920	1.9840	1.9840	1.9898	1.9796	1.9796
TAE	1.9686	1.9381	1.9381	1.8787	1.7722	1.7722	1.8902	1.7925	1.7925
VDE	1.9850	1.9702	1.9702	1.9947	1.9894	1.9894	1.8469	1.7172	1.7172
BioEMU-CV	1.9719	1.9446	1.9446	1.9939	1.9878	1.9878	1.9859	1.9721	1.9721

### C.5 SIMPLE BASELINES

**Experiment setup.** Here, we show that simple baselines, e.g., PCA and TICA, on  $C_\alpha$ -wise distance fail for Trp-cage. We use the first principal component and the first time-lagged principal component as CVs. All other details are identical; the training data is for the baseline and BIOEMU-CV, normalization to the range [-1, 1] over the whole DESRES trajectory data.

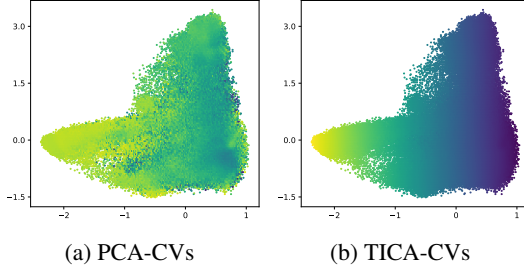


Figure 14: **Simple method CVs on TICA projections of the full DESRES trajectory.** PCA-CVs fails to discriminate the folded and unfolded state, while TICA-CVs obviously shows correlation with the TICA using the full DESRES trajectory.

**Qualitative results.** In Figure 14, we color TICA plot with the CVs. Since the axes were computed with TICA on the full DESRES dataset, TICA-CVs show high correlation with the  $x$  axis. Nonetheless, PCA-CVs show meaningless values in Trp-cage compared to MLCVs in Figure 6, failing to discriminate between the folded and unfolded state.

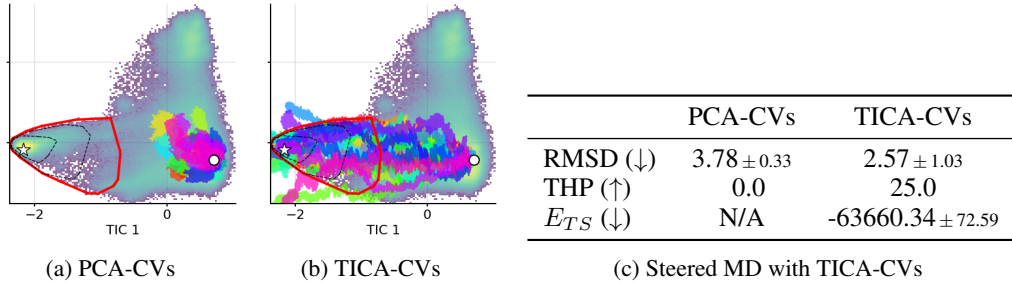


Figure 15: **Visualization of transition paths and quantitative results of steered MD.** PCA-CVs fails to reach the target state, where TICA-CVs sometimes reach the target state with a low energy.

**Steered MD results.** For steered MD, we identically mix with the  $C_\alpha$  RMSD CVs in a ratio of 5:5, as for our baselines and BIOEMU-CV. In Figure 15, PCA-CVs fail to reach the target state, while TICA-CVs often reach the target state with low energy. However, its THP is low compared to baselines, failing to find meaningful transition pathways.

### C.6 CAPTURING MULTI-PATHWAYS IN ALANINE DIPEPTIDE

Here, we test CVs from time-lagged generation for capturing multi-pathways in Alanine Dipeptide.

**Alanine Dipeptide.** Alanine Dipeptide is a well-studied molecule consisting of 22 atoms with two optimal CVs: the backbone dihedral angles  $\phi$  and  $\psi$ . We use two meta-stable states  $C5$  and  $C7_{ax}$ , each located at  $(-2.49, 2.67)$  and  $(1.02, -0.70)$  in  $(\phi, \psi)$ . Typically, two pathways are known to pass near each saddle point in the energy barrier at  $\phi = 0$  (Holdijk et al., 2023; Seong et al., 2025). Training data were randomly extracted from 10 ns molecular dynamics trajectories with amber99sbildn force field and tip3p implicit solvent by OpenMM (Eastman et al., 2023) for a fair comparison, with five trajectories each initialized in the  $C5$  and  $C7_{ax}$  meta-stable state. We train from scratch with time-lagged conditioning, since the released weights were obtained from a different force field. Among data pairs  $(x_t, x_{t+\tau})$ , no transition events exists.

**Experiment setup.** We use the Transferable Boltzmann Generators (Klein & Noé, 2024, TBG) architecture for the generative backbone model, namely TBG-CV. For time-lagged conditioning, MLCVs were concatenated to the node feature of GNNs. DeepTICA and TAE used heavy atom distances as stated, while VDE and TBG-CV used heavy atom coordinates with Kabsch alignment (Kabsch, 1976) for invariance. The autocorrelation loss from VDE was applied to stabilize the training. The number of parameters of encoders were all identical, with the same training configuration under the `mlcolvar` library (Bonati et al., 2023).

**OPES simulation results.** Meta-stable basins were defined as  $\phi > 0$  and  $\phi < 0$ , using the known optimal CVs. The first 3 ns of the OPES simulations were discarded, with  $\Delta F$  updated every 1 ns. In Table 11, most simulations converge close to the reference free energy difference value obtained by using dihedral angles as CVs, while TAE exhibits a relatively high variance.

**Steered molecular dynamics results.** We define the target hit region by dihedral angles, and steer 256 paths by only MLCVs, with  $k$  searched for a hundred units. In Table 11, TBG-CV outperforms other MLCVs with high THP and low  $E_{TS}$ , and shows pathways crossing near the saddle points in the energy barrier in Figure 16, while baselines mostly ignore the energy landscape.

Table 11: **Quantitative results of 20 ns OPES simulations and steered MD on Alanine Dipeptide.** Free energy difference values within the range of 1.25 kJ/mol from the reference are considered to success. RMSD and THP are averaged over all trajectories, while max energy ( $E_{TS}$ ) is averaged over trajectories only hitting the target state. Best results are highlighted in **bold** and second in underline in Steered MD.

Method	OPES			SMD		
	SIGMA	$\Delta F$	$k$	RMSD ( $\downarrow$ ) Å	THP ( $\uparrow$ ) %	$E_{TS} (\downarrow)$ kJmol $^{-1}$
Ref $(\phi, \psi)$	0.05	$10.06 \pm 0.22$	200	1.0640	100.00	$-3.89 \pm 5.80$
DeepTICA	0.10	$9.99 \pm 0.21$	400	0.9729	8.59	$814.52 \pm 115.74$
TAE	0.05	$9.22 \pm 1.74$	1200	1.0086	<u>58.59</u>	<u><math>755.41 \pm 92.30</math></u>
VDE	0.05	$10.11 \pm 0.28$	700	<b>0.8582</b>	5.08	$901.69 \pm 115.59$
TBG-CV	0.05	$9.83 \pm 1.15$	300	<u>0.9593</u>	<b>60.93</b>	<b><u>33.58</u> ± 15.19</b>

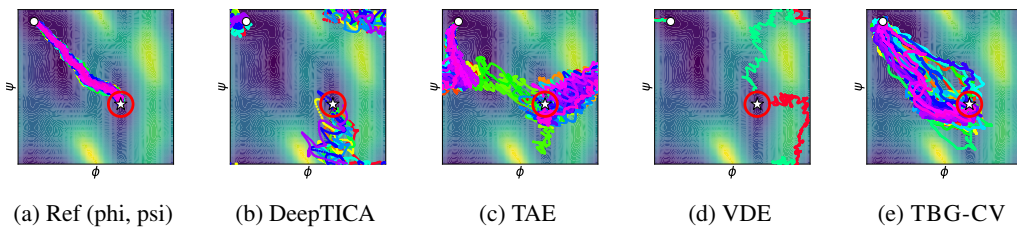


Figure 16: **Visualization of hitting pathways from steered MD.** Initial state  $C5$  and target state  $C7_{ax}$  are each denoted as white circles and stars, and the red circle indicates the target hit region.

### C.7 HIGH-DIMENSIONAL CVS

Here, we show qualitative results of extending CVs to higher dimensions, bigger than one. We train an encoder with four-dimensional CVs on BBA, with all other configurations identical.

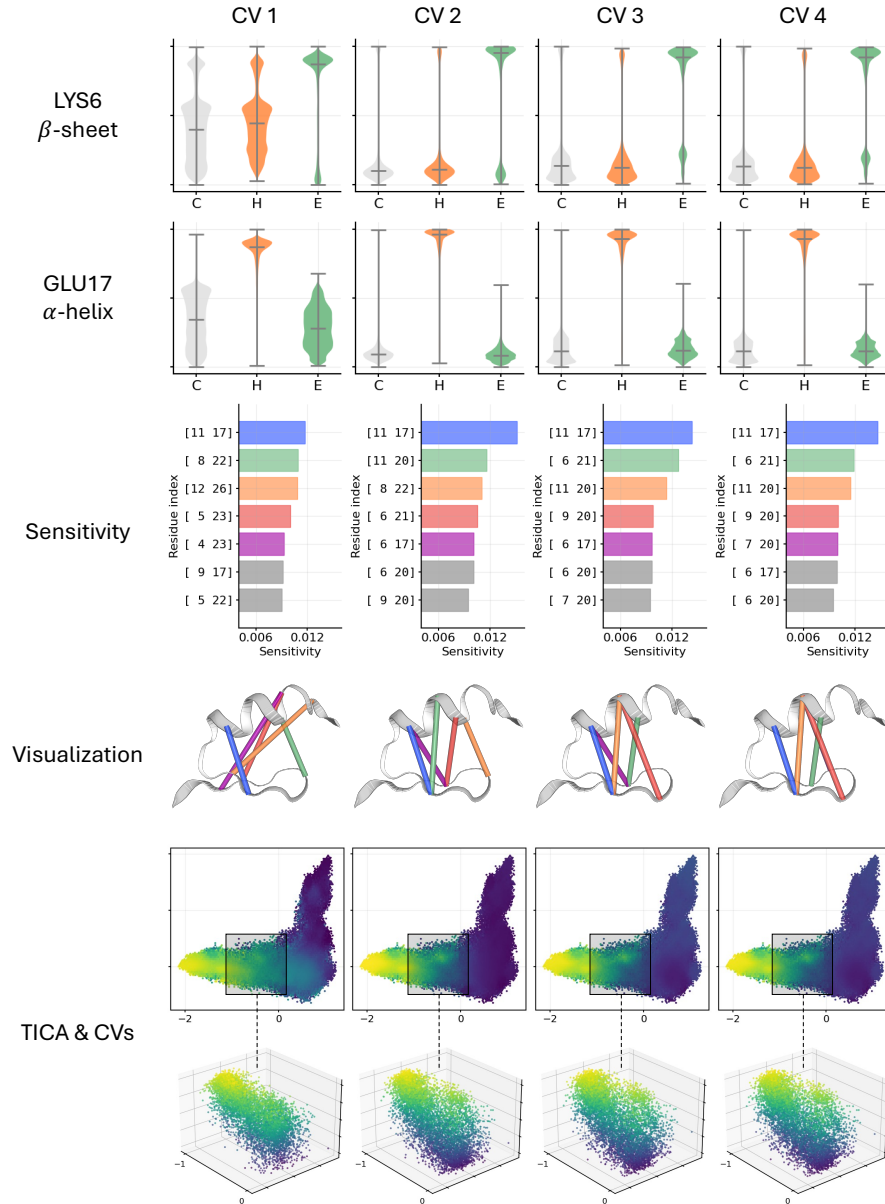


Figure 17: **Qualitative results of multi dimension CVs on BBA.** From top to bottom, we plot the secondary structure violin plot for two residues, sensitivity analysis, visualization of sensitivity in the folded structure, and TICA plots colored by the CV value.

In Figure 17, we visualize all the analyses used in the main paper for each dimension of the CVs. While all CVs are most sensitive to the 11th and 17th residue, other sensitivities differ, indicating each dimension is looking at different input descriptors and shows a different detailed slow degree of freedom. Furthermore, the secondary structures and TICA plots between the first and other dimensions differ. Overall, the first dimension shows distinct behavior compared to other dimensions.

### C.8 LONGER SIMULATION RESULTS

Here, we report the results of longer OPES simulations. To be specific, we report 9829 ns  $\approx 9.8 \mu\text{s}$  length simulation for Trp-cage using DeepTICA, computed on four RTX 3090 GPUs for one month.

Table 12: **Quantitative results of long OPES simulation on Trp-cage with DeepTICA MLCVs.**

Time horizon	$\Delta F_{ref}$	$\Delta F$	$ \Delta F_{ref} - \Delta F  (\downarrow)$	PMF MAE ( $\downarrow$ )
1 $\mu\text{s}$		$6.53 \pm 7.31$	2.73	$8.94 \pm 7.43$
9.8 $\mu\text{s}$	3.70	$-3.36 \pm 2.76$	7.60	$7.64 \pm 3.81$

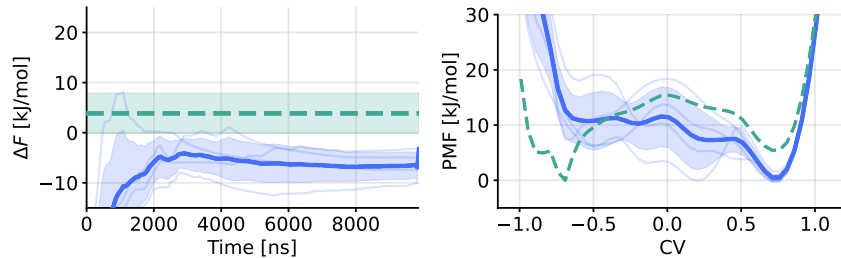


Figure 18: **Free energy (left) and PMF (right) estimation from  $9.8 \mu\text{s}$  OPES simulations for Trp-cage with DeepTICA MLCVs.** Green dotted lines indicated the reference value, and blue lines refer to the free energy difference during the OPES simulations. Solid line refer to the mean, and shaded areas are standard deviation.

As seen in Table 12 and Figure 18, simulations with approximately ten times longer results do not fully converge and still exhibit uncertainty. While the folded state is sampled many times, the unfolded states are not sampled properly, resulting in a gap in the negative range of CVs in the PMF plot. Overall, longer OPES evaluations do not provide more meaningful insights.

## D ABLATION EXPERIMENTS RESULTS

In this section, we present various ablation experiments on BIOEMU-CV.

### D.1 TIME-LAGGED CONDITIONING AND FIXED BIOEMU WEIGHTS

Here, we conduct ablation experiment on not using time-lagged conditions and unfreezing BioEmu’s parameters, with OPES simulations and Steered MD.

**Table 13: Ablation experiments for the components of BIOEMU-CV in OPES and steered MD simulations.** Time-lag indicates whether the model is trained to generated a time-lagged target conformation, and freezing indicates whether BioEmu’s parameters are kept fixed during the training of the encoder. Our current design choice shows high performance for SMD results.

Components		OPES simulations				Steered MD		
Time-lag	Freezing	$\Delta F_{\text{ref}}$	$\Delta F$	$ \Delta F_{\text{ref}} - \Delta F  (\downarrow)$	PMF MAE ( $\downarrow$ )	RMSD ( $\downarrow$ ) Å	THP ( $\uparrow$ ) %	$E_{TS} (\downarrow)$ kJ/mol
✓	✓	-3.71	$-3.19 \pm 3.97$	0.52	$3.07 \pm 2.53$	<b>1.20 ± 0.33</b>	<b>100.0</b>	$-82055.15 \pm 98.48$
✗	✓	-3.68	$-5.78 \pm 3.20$	2.10	$1.41 \pm 1.56$	$1.57 \pm 0.36$	81.3	$-82084.68 \pm 62.86$
✓	✗	-4.47	$-3.25 \pm 0.81$	1.22	$3.53 \pm 3.73$	$1.62 \pm 0.31$	<b>100.0</b>	$-82076.42 \pm 98.20$

**Time-lagged conditioning.** We input a conformation  $x_t$  to the MLCV encoder, and condition the BioEmu to generate  $x_t$  instead of using time-lagged data  $x_{t+\tau}$ . Formally, we are testing the denoising score-matching objective modified from Equation (1) as follows:

$$\mathcal{L}(x_t, A) = \mathbb{E}_{s \sim \mathcal{U}[0,1]} \left[ \lambda_s \left\| \nabla \log p_{s|0} \left( x_t^{(s)} | x_t^{(0)}, x_t, A \right) - g_\phi(s, h_t, z) \right\|^2 \right].$$

In Table 13, one can see that time-lagged conditioning results in a better performance for both downstream tasks, i.e., OPES and steered MD simulations. Intuitively, time-lagged data will inject dynamic information into the MLCVs, resulting enrich representations.

**Unfrozen BioEmu weights.** We also test whether unfreezing the BioEmu parameters would improve performance, while BIOEMU-CV only trains the parameters of the MLCV encoder. In Table 13, MLCV trained with a frozen BioEmu results in a lower RMSD in SMD and better OPES results. Since the performance is slightly better in unfrozen cases, keeping the lightweight training scheme is reasonable.

## D.2 ENCODER SIZES AND PLACEMENT

Table 14: **Quantitative results of steered MD for different encoder sizes.** The performance remains largely unchanged across the encoder size.

Param.	Repr.	RMSD ( $\downarrow$ ) Å	THP ( $\uparrow$ ) %	$E_{TS}$ ( $\downarrow$ ) kJ/mol
48K	single	<b>1.20 ± 0.33</b>	<b>100.0</b>	-82055.15 ± 98.48
1.27M	single	1.50 ± 0.30	100.0	-82071.13 ± 100.08
196K	single	<u>1.41 ± 0.32</u>	<u>93.8</u>	-82049.40 ± 98.52
48K	pair	1.79 ± 0.45	56.3	<b>-82088.33 ± 76.61</b>
48K	single, pair	1.66 ± 0.56	68.8	-82086.61 ± 74.80

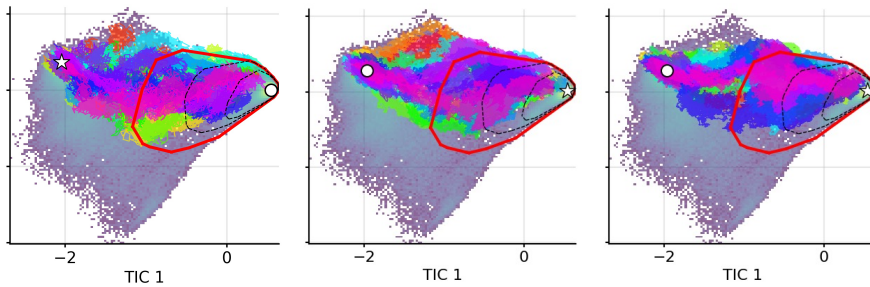


Figure 19: **Qualitative results of steered MD for different encoder sizes.** From left to right, each visualizes the paths from the steered MD from the encoder with 48K, 196K, and 1.27M parameters.

**Encoder size.** We test 48K, 196K, 1.27M parameters with layers  $\{2, 4, 8\}$  and hidden dimension  $\{100, 200, 400\}$  for Chignolin, where the main paper encoder corresponds to the 48K parameter setting. All MLCVs were mixed with  $C_\alpha$  RMSD CVs at a 5:5 ratio. In Figure 19 and Table 14, performance remains largely unchanged across the encoder size. Since the encoder is inferred millions of times during the OPES simulation, keeping a relatively smaller size would be practical.

**Conditioning placement.** Additionally, we test whether on how selecting the conditioning representation affects on the performance. While BIOEMU-CV conditions the single representation as  $h_t = \text{MLP}(h, c_t)$ , we additionally test conditioning the pair representation, i.e.,  $z_t = \text{MLP}(z, c_t)$  and both the single and pair representation. In Table 14, RMSD and THP both fall behind the case of only conditioning the single representation, while the energy shows little improvement.

## D.3 STEERED MD WITHOUT MIXING CVs

**Table 15: Ablation experiments of steered molecular dynamics on three fast-folding proteins in explicit water solvent, without  $C_\alpha$ -RMSD CVs.** We mark not applicable (N/A) for CVs that fail at state discrimination and trajectories not arriving at the target meta-stable state.

Molecule	$k$	Method	RMSD ( $\downarrow$ ) Å	THP ( $\uparrow$ ) %	$E_{TS}$ ( $\downarrow$ ) kJ/mol
Chignolin	1000	DeepTICA	$7.24 \pm 1.49$	0.0	N/A
		TAE	$5.72 \pm 1.94$	6.2	$-81951.53 \pm 0.00$
		VDE	N/A	N/A	N/A
		BIOEMU-CV	$7.82 \pm 1.47$	0.0	N/A
	2000	DeepTICA	$7.01 \pm 1.71$	0.0	N/A
		TAE	$6.39 \pm 1.74$	0.0	N/A
		VDE	N/A	N/A	N/A
		BIOEMU-CV	$6.09 \pm 2.21$	6.2	$-82023.05 \pm 0.00$
Trp-cage	2000	DeepTICA	$2.23 \pm 1.23$	0.0	N/A
		TAE	$8.62 \pm 3.25$	0.0	N/A
		VDE	N/A	N/A	N/A
		BIOEMU-CV	$12.17 \pm 1.58$	0.0	N/A
	5000	DeepTICA	$10.78 \pm 1.15$	0.0	N/A
		TAE	$7.22 \pm 1.71$	0.0	N/A
		VDE	N/A	N/A	N/A
		BIOEMU-CV	$7.14 \pm 1.52$	0.0	N/A
BBA	50000	DeepTICA	$7.39 \pm 2.71$	0.0	N/A
		TAE	$9.87 \pm 1.59$	0.0	N/A
		VDE	N/A	N/A	N/A
		BIOEMU-CV	$6.03 \pm 2.56$	0.0	N/A
	100000	DeepTICA	N/A	N/A	N/A
		TAE	$10.20 \pm 1.59$	0.0	N/A
		VDE	N/A	N/A	N/A
		BIOEMU-CV	$6.64 \pm 1.95$	0.0	N/A

**Steered MD without  $C_\alpha$ -RMSD CVs.** Here, we report the performance of steered MD using MLCVs without  $C_\alpha$  RMSD. In Table 15, MLCV steered MD mostly fails to reach the target. The force constant  $k$  was set to the maximum value with simulations not exploding, resulting in different  $k$  values compared to Table 2. Due to this, we have incorporated  $C_\alpha$  RMSD for all MLCVs in Table 2.